Synthesis and Characterization of Quinone-Substituted Octaalkyl Porphyrin Monomers and Dimers

Jonathan L. Sessler,*,† Martin R. Johnson,† Stephen E. Creager,† James C. Fettinger,‡ and James A. Ibers*,‡

Contribution from the Departments of Chemistry, University of Texas at Austin, Austin, Texas 78712, and Northwestern University, Evanston, Illinois 60208.
Received April 17, 1990

Abstract: The synthesis and characterization of a variety of selectively metalated quinone-substituted zinc-containing octaalkyl porphyrin dimers, designed to mimic certain key electronic and structural aspects of the photosynthetic reaction centers of *Rhodopseudomonas viridis* and *Rhodobacter sphaeroides*, and appropriate control monomers and dimers are described. These new compounds have been characterized by ^{1}H NMR, ^{13}C NMR, UV-visible spectroscopy, mass spectrometry, and microanalysis. Electrochemical data are also given for representative dimers and monomers and X-ray structural information is provided for a 1,3-phenyl-linked and a 1,4-phenyl-linked functionalized copper-containing dimer (Cu_2·**5** and Cu_2·**9**, respectively) and for a quinone-substituted metal-free monomer (H_2·**20**). Crystallographic data for H_2·**20** is as follows: monoclinic, $P2_1/c$, a = 8.241 (6), b = 30.34 (3), c = 13.502 (12) Å, β = 92.86 (1)°, t = −162 °C, Z = 4, $R(F)$ = 0.069, NV = 434, NO = 5894. Crystallographic data for Cu_2·**5**·(1.5$CHCl_3$)·(0.5CH_3OH) is as follows: triclinic, $P\bar{1}$, a = 19.015 (4), b = 19.043 (6), c = 12.957 (5) Å, α = 109.90 (2)°, β = 108.84 (2)°, γ = 101.86 (2)°, t = −162 °C, Z = 2, $R(F)$ = 0.085, NV = 1015, NO = 11574. Crystallographic data for Cu_2·**9**·(2$CHCl_3$) is as follows: triclinic, $P\bar{1}$, a = 12.036 (3), b = 12.762 (3), c = 14.353 (3) Å, α = 94.64 (1)°, β = 103.54 (1)°, γ = 104.68 (1)°, t = −115 °C, Z = 1 (molecule has a crystallographically imposed center of symmetry), $R(F)$ = 0.067, NV = 505, NO = 8318.

At present, the bacterial photosynthetic reaction centers are the only membrane-bound electron-transfer proteins for which highly refined crystal structures exist. Thus, much of our current understanding of complex *multi step* electron transfer processes derives from studies of these systems.[1] To date, two reaction centers, those from *Rhodopseudomonas viridis*[2] and *Rhodobacter sphaeroides*,[3] have been characterized structurally. Six tetrapyrrolic subunits are found at these two very similar active sites: A dimeric bacteriochlorophyll "special pair" (P), two "accessory" bacteriochlorophylls (Bchls), and two bacteriopheophytins (Bphs), all held in a well-defined but skewed geometry along a C_2 axis of symmetry. The Bchls are separated from the P by center-to-center distances of ca. 11 Å and interplane angles of ca. 70°. The Bphs in turn are separated by similar distances and angles from the Bchls. Four of these six prosthetic groups are currently considered to define the relevant electron transport chain.[1c,4,5] This consists in sequence of the P photosensitizer, an "accessory" Bchl, an intermediate Bph, and a quinone acceptor (Q). In *R. sphaeroides*, Q is an ubiquinone; in *R. viridis*, it is a menaquinone. In both cases, Q lies roughly 13-14 Å away from the corresponding Bph center. Charge separation between the P* and Bph entities is known to occur on a time scale of 2-4 ps[6-9] with nearly 100% quantum efficiency.[1b,c] Furthermore this process exhibits activationless behavior, increasing in rate by a factor of 2 at liquid helium temperature.[6,10] The resulting P^+-Bchl-Bph^- charge-separated state can exist stably for a long period of time; in the normal course of events in vivo, a subsequent irreversible electron transfer to give P^+-Bchl-Bph-Q^- occurs in 200 ps, also with 100% quantum yield.[1c]

In spite of the availability of the above structural and kinetic information, many mechanistic aspects of bacterial photosynthesis, including the rapid, activationless, and efficient nature of the initial charge separation process, remain poorly understood.[1] One of the most significant issues currently being debated concerns the role of the "intermediate" or "accessory" Bchl. Recent subpicosecond transient absorption experiments have failed to provide any evidence that a P^+-$Bchl^-$ state acts as a discrete intermediate in the initial P*-Bchl-Bph → P^+-Bph-Bph^- charge separation process.[6-9] Nonetheless, it seems unlikely that the electron traverses the ca. 10 Å edge-to-edge distance from the P to the Bph in a few picoseconds without the Bchl playing an important role. One explanation, which has been formulated in various guises[11] and for which some experimental evidence has recently been presented,[12] involves a two-step sequential electron transfer, in which an intermediate $Bchl^-$ (or Bph^+) species is actually formed but is not observable, decaying faster than it is observed. Another alternative is that the Bchl facilitates transfer to the Bph via a "superexchange" mechanism that involves a quantum mechanical mixing of a virtual P^+-$Bchl^-$ state with the photoexcited dimer, P*.[13-15] There has been much controversy (but no definitive

† University of Texas at Austin.
‡ Northwestern University.

(1) For reviews, see: (a) Marcus, R. A.; Sutin, N. *Biochim. Biophys. Acta* **1985**, *811*, 265-322. (b) Windsor, M. W. *J. Chem. Soc. Farad. Trans. 2* **1986**, *82*, 2237-2243. (c) Kirmaier, C.; Holten, D. *Photosyn. Res.* **1987**, *13*, 225-260. (d) Feher, G.; Allen, J. P.; Okamura, M. Y.; Rees, D. C. *Nature* **1989**, *339*, 111-116. (e) Huber, R. *Angew. Chem., Int. Ed. Engl.* **1989**, *28*, 848-869.

(2) (a) Deisenhofer, J.; Epp, O.; Miki, K.; Huber, R.; Michel, H. *J. Mol. Biol.* **1984**, *180*, 385-398. (b) Deisenhofer, J.; Epp, O.; Miki, K.; Huber, R.; Michel, H. *Nature* **1985**, *318*, 618-624. (c) Deisenhofer, J.; Michel, H. *Angew. Chem., Int. Ed. Engl.* **1989**, *28*, 829-847.

(3) (a) Chang, C.-H.; Schiffer, M.; Tiede, D.; Smith, U.; Norris, J. *J. Mol. Biol.* **1985**, *186*, 201-203. (b) Allen, J. P.; Feher, G.; Yeates, T. O.; Komiya, H.; Rees, D. C. *Proc. Natl. Acad. Sci. U.S.A.* **1987**, *84*, 5730-5734. (c) Allen, J. P.; Feher, G.; Yeates, T. O.; Komiya, H.; Rees, D. C. *Proc. Natl. Acad. Sci. U.S.A.* **1987**, *84*, 6162-6166.

(4) Kirmaier, C.; Holten, D.; Parson, W. W. *Biochim. Biophys. Acta* **1985**, *810*, 49-61.

(5) Bocian, D. F.; Boldt, N. J.; Chadwick, B. W.; Frank, H. A. *FEBS Lett.* **1987**, *214*, 92-96.

(6) Woodbury, N. W.; Becker, M.; Middendorf, D.; Parson, W. W. *Biochemistry* **1985**, *24*, 7516-7521.

(7) (a) Martin, J.-L.; Breton, J.; Hoff, A. J.; Migus, A.; Antonetti, A. *Proc. Natl. Acad. Sci. U.S.A.* **1986**, *83*, 957-961. (b) Breton, J.; Martin, J.-L.; Migus, A.; Antonetti, A.; Orszag, A. *Proc. Natl. Acad. Sci. U.S.A.* **1986**, *83*, 5121-5125. (c) Breton, J.; Martin, J.-L.; Fleming, G. R.; Lambry, J.-C. *Biochemistry* **1988**, *27*, 8276-8284.

(8) Wasielewski, M. R.; Tiede, D. M. *FEBS Lett.* **1986**, *204*, 368-372.

(9) Kirmaier, C.; Holten, D. *FEBS Lett.* **1988**, *239*, 211-218.

(10) Fleming, G. R.; Martin, J. L.; Breton, J. *Nature* **1988**, *333*, 190-192.

(11) (a) Fischer, S. F.; Scherer, P. O. J. *Chem. Phys.* **1987**, *115*, 151-158. (b) Marcus, R. A. *Chem. Phys. Lett.* **1988**, *146*, 13-22.

(12) Holzapfel, W.; Finkele, U.; Kaiser, W.; Oesterhelt, D.; Scheer, H.; Stilz, H. U.; Zinth, W. *Chem. Phys. Lett.* **1989**, *160*, 1-7.

(13) Marcus, R. A. *Chem. Phys. Lett.* **1987**, *133*, 471-477.

0002-7863/90/1512-9310$02.50/0 © 1990 American Chemical Society

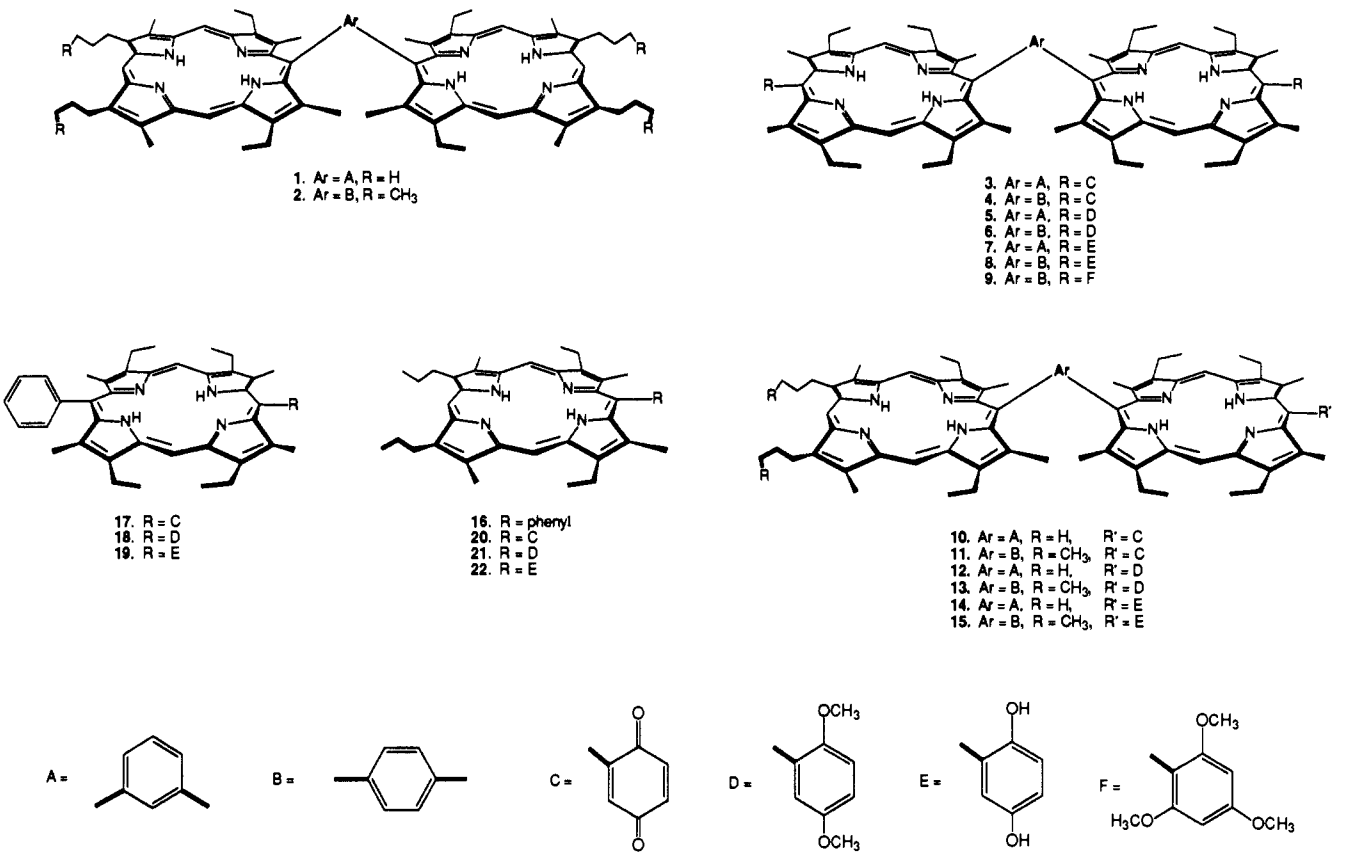

Figure 1. New porphyrins prepared for this study. In the text, a simple bold-face number is used to refer to the generalized forms of these compounds, whereas the prefixes H_2, Zn, and Cu are used to denote, respectively, the free-base, zinc(II), and copper(II) forms of each porphyrin monomer or dimer subunit. Thus, for instance, a designation H_2Zn-**10** refers to the monozinc complex of the free-base dimer H_4-**10** in which the zinc(II) cation is bound in the porphyrin macrocycle adjacent (or "proximal") to the quinone subunit, whereas the designation ZnH_2-**10** refers to the corresponding regioisomer in which the single zinc(II) cation is bound in the porphyrin distant (or "distal") from the quinone.

resolution) as to whether this latter mechanism is consistent with all the available experimental observations and, as a result, extensive experimental and theoretical efforts continue. Another potentially informative approach involves the study of suitable model systems.

In recent years, many model compounds have been prepared in an effort to understand further the natural photosynthetic systems.[16] Some of these, such as porphyrin-free donor-acceptor dimers,[17,18] bicyclooctane-bridged systems,[19,20] and capped systems,[21-26] as well as numerous other linked systems,[27-29] have proved useful in exploring how various factors, such as dis-

(14) (a) Bixon, M.; Jortner, J.; Michel-Beyerle, M. E.; Ogrodnik, A.; Lersch, W. *Chem. Phys. Lett.* **1987**, *140*, 626–630. (b) Michel-Beyerle, M. E.; Bixon, M.; Jortner, J. *Chem. Phys. Lett.* **1988**, *151*, 188–194. (c) Plato, M.; Möbius, K.; Michel-Beyerle, M. E.; Bixon, M.; Jortner, J. *J. Am. Chem. Soc.* **1988**, *110*, 7279–7285. (d) Bixon, M.; Jortner, J. *Chem. Phys. Lett.* **1989**, *159*, 17–20. (e) Boxer, S. G.; Goldstein, R. A.; Lockhart, D. J.; Middendorf, T. R.; Takiff, L. *J. Phys. Chem.* **1989**, *93*, 8280–8294.

(15) (a) Won, Y.; Friesner, R. A. *Proc. Natl. Acad. Sci. U.S.A.* **1987**, *84*, 5511–5515. (b) Won, Y.; Friesner, R. A. *Biochim. Biophys. Acta* **1988**, *935*, 9–18. (c) Friesner, R. A.; Won, Y. *Biochim. Biophys. Acta* **1989**, *977*, 99–122.

(16) For recent reviews, see: (a) Wasielewski, M. R. *Photochem. Photobiol.* **1988**, *47*, 923–929. (b) Gust, D.; Moore, T. A. *Science* **1989**, *244*, 35–41. (c) Connolly, J. S.; Bolton, J. R. In *Photoinduced Electron Transfers*; Fox, M. A., Channon, M., Eds.; Elsevier: Amsterdam, 1988; Part D, Chapter 6.2, pp 303–393. For reviews of earlier work, see: (a) Fendler, J. H. *J. Phys. Chem.* **1985**, *89*, 2730–2740. (b) Boxer, S. G. *Biochim. Biophys. Acta* **1983**, *726*, 265–292. See also: *Tetrahedron* **1989**, *45*(*15*) (a special "Symposium in Print" issue devoted to the topic of covalently linked donor-acceptor photosynthetic model systems, Gust, D., Moore, T. A., Eds.).

(17) (a) Miller, J. R.; Calcaterra, L. T.; Closs, G. L. *J. Am. Chem. Soc.* **1984**, *106*, 3047–3049. (b) Miller, J. R.; Beitz, J. V.; Huddleston, R. K. *J. Am. Chem. Soc.* **1984**, *106*, 5057–5068. (c) Closs, G. L.; Calcaterra, T. L.; Green, N. J.; Penfield, K. W.; Miller, J. R. *J. Phys. Chem.* **1986**, *90*, 3673–3683. (d) Penfield, K. W.; Miller, J. R.; Paddon-Row, M. N.; Cotsaris, E.; Oliver, A. M.; Hush, N. S. *J. Am. Chem. Soc.* **1987**, *109*, 5061–5065. (e) Closs, G. L.; Piotrowiak, P.; MacInnis, J. M.; Fleming, G. R. *J. Am. Chem. Soc.* **1988**, *110*, 2652–2653. (f) Closs, G. L.; Miller, J. R. *Science* **1988**, *240*, 440–447. (g) Closs, G. L.; Johnson, M. D.; Miller, J. R.; Piotrowiak, P. *J. Am. Chem. Soc.* **1989**, *111*, 3751–3753. (h) Johnson, M. D.; Miller, J. R.; Green, N. S.; Closs, G. L. *J. Phys. Chem.* **1989**, *93*, 1173–1176.

(18) (a) Pasman, P.; Rob, F.; Verhoeven, J. W. *J. Am. Chem. Soc.* **1982**, *104*, 5127–5133. (b) Heitele, H.; Michel-Beyerle, M. E. *J. Am. Chem. Soc.* **1985**, *107*, 8286–8288. (c) Warman, J. M.; De Haas, M. P.; Oevering, H.; Verhoeven, J. W.; Paddon-Row, M. N.; Oliver, A. M.; Hush, N. S. *Chem. Phys. Lett.* **1986**, *128*, 95–99. (d) Oevering, H.; Verhoeven, J. W.; Paddon-Row, M. N.; Costaris, E.; Hush, N. S. *Chem. Phys. Lett.* **1988**, *143*, 488–495.

(19) (a) Joran, A. D.; Leland, B. A.; Geller, G. G.; Hopfield, J. J.; Dervan, P. B. *J. Am. Chem. Soc.* **1984**, *106*, 6090–6092. (b) Leland, B. A.; Joran, A. D.; Felker, P. M.; Hopfield, J. J.; Zewail, A. H.; Dervan, P. B. *J. Phys. Chem.* **1985**, *89*, 5571–5573. (c) Joran, A. D.; Leland, B. A.; Felker, P. M.; Zewail, A. H.; Hopfield, J. J.; Dervan, P. B. *Nature* (*London*) **1987**, *327*, 508–511. (d) Joran, A. D. Doctoral Dissertation, California Institute of Technology, 1986. (e) Leland, B. A. Doctoral Dissertation, California Institute of Technology, 1987.

(20) Bolton, J. R.; Ho, T.-F.; Liauw, S.; Siemiarczuk, A.; Wan, C. S. K.; Weedon, A. C. *J. Chem. Soc., Chem. Commun.* **1985**, 559–560.

(21) (a) Weiser, J.; Staab, H. A. *Angew. Chem., Int. Ed. Engl.* **1984**, *23*, 623–625. (b) Krieger, C.; Weiser, J.; Staab, H. A. *Tetrahedron Lett.* **1985**, 6055–6058. (c) Weiser, J.; Staab, H. A. *Tetrahedron Lett.* **1985**, 6059–6062. (d) Mauzerall, D.; Weiser, J.; Staab, H. *Tetrahedron* **1989**, *45*, 4807–4814.

(22) Morgan, B.; Dolphin, D. *Angew. Chem., Int. Ed. Engl.* **1985**, *24*, 1003–1004.

(23) (a) Lindsey, J. S.; Mauzerall, D. C. *J. Am. Chem. Soc.* **1982**, *104*, 4498–4500. (b) Lindsey, J. S.; Mauzerall, D. C.; Linschitz, H. *J. Am. Chem. Soc.* **1983**, *105*, 6528–6529. (c) Lindsey, J. S.; Delaney, J. K.; Mauzerall, D. C.; Linschitz, H. *J. Am. Chem. Soc.* **1988**, *110*, 3610–3621. (d) Delaney, J. K.; Mauzerall, D. C.; Lindsey, J. S. *J. Am. Chem. Soc.* **1990**, *112*, 957–963.

(24) (a) Leighton, P.; Sanders, J. K. M. *J. Chem. Soc., Chem. Commun.* **1985**, 24–25. (b) Irvine, M. P.; Harrison, R. J.; Beddard, G. S.; Leighton, P.; Sanders, J. K. M. *Chem. Phys.* **1986**, *104*, 315–324. (c) Harrison, R. J.; Pearce, B.; Beddard, G. S.; Cowan, J. A.; Sanders, J. K. M. *Chem. Phys.* **1987**, *116*, 429–448.

(25) (a) Osuka, A.; Furuta, H.; Maruyama, K. *Chem. Lett.* **1986**, 479–482. (b) Osuka, A.; Maruyama, K. *J. Chem. Res.* (*S*) **1987**, 286–287. (c) Osuka, A.; Maruyama, K.; Hirayama, S. *Tetrahedron* **1989**, *45*, 4815–4830.

Scheme I. Synthesis of Pyrrolic Precursors

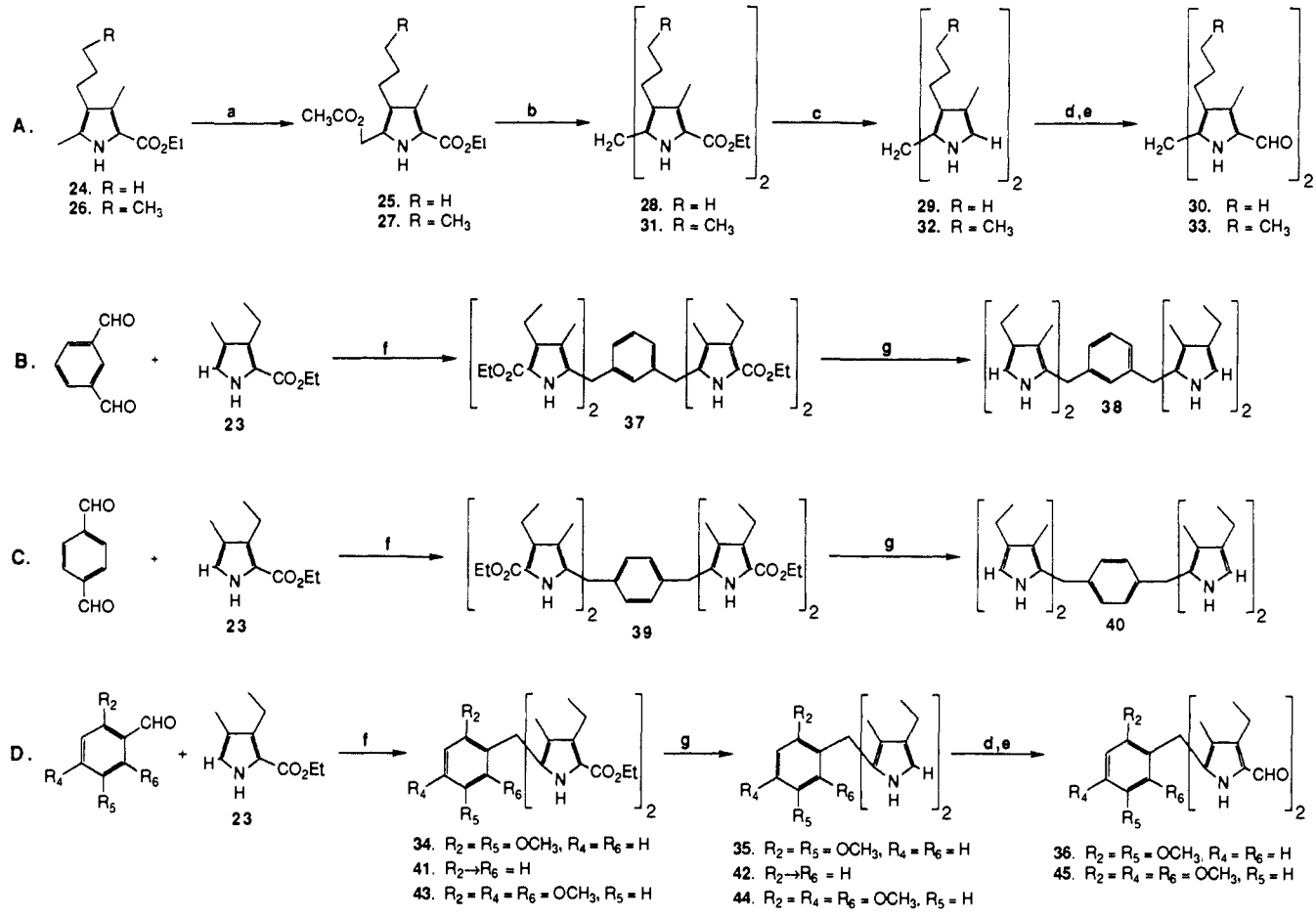

Reagents: (a) $Pb(OAc)_4$/HOAc. (b) HCl/90% EtOH/reflux. (c) NaOH/H_2O/reflux. (d) $POCl_3$/DMF/-20 to 0 °C. (e) H_2O/NaOH. (f) HCl/95% EtOH/reflux. (g) NaOH/$(CH_2OH)_2$/180-195 °C.

tance,[19-25] donor-acceptor orientation[28c] and energetics,[19c,24,29b] and solvent[20,24,27,28b,29b] mediate photoinduced electron-transfer reactions. Other models,[30-32] such as triads[30] and triptycene-derived systems,[31] exhibit interesting charge separation properties. In all cases, however, there are substantial differences between the models and the actual reaction centers. Indeed, with rare exceptions,[33-36] *all* the photosynthetic model systems reported to date have consisted of a simple *monomeric* porphyrin substituted with one or more acceptors,[37] and none, to our knowledge, has

(26) (a) Sanders, G. M.; van Dijk, M.; van Veldhuizen, A.; van der Plas, H. C.; Koning, G. P. *Recueil* **1985**, *104(9)*, 243-244. (b) Sanders, G. M.; van Dijk, M.; van Veldhuizen, A.; van der Plas, H. *J. Chem. Soc., Chem. Commun.* **1986**, 1311-1313.

(27) (a) Siemiarczuk, A.; McIntosh, A. R.; Ho, T.-F.; Stillman, M. J.; Roach, K. J.; Weedon, A. C.; Bolton, J. R.; Connolly, J. S. *J. Am. Chem. Soc.* **1983**, *105*, 7224-7230. (b) Schmidt, J. A.; Siemiarczuk, A.; Weedon, A. C.; Bolton, J. R. *J. Am. Chem. Soc.* **1985**, *107*, 6112-6114. (c) Hofstra, U.; Schaafsma, T. J.; Sanders, G. M.; Van Dijk, M.; Van der Plas, H. C.; Johnson, D. G.; Wasielewski, M. R. *Chem. Phys. Lett.* **1988**, *151*, 169-175. (d) Schmidt, J. A.; McIntosh, A. R.; Weedon, A. C.; Bolton, J. R.; Connolly, J. S.; Hurley, J. K.; Wasielewski, M. R. *J. Am. Chem. Soc.* **1988**, *110*, 1733-1740 and references cited therein.

(28) (a) Migita, M.; Okada, T.; Mataga, N.; Nishitani, S.; Kurata, N.; Sakata, Y.; Misumi, S. *Chem. Phys. Lett.* **1981**, *84*, 263-266. (b) Mataga, N.; Karen, A.; Okada, T.; Nishitani, S.; Kurata, Sakata, Y.; Misumi, S. *J. Phys. Chem.* **1984**, *88*, 5138-5141. (c) Baumannn, W.; Frohling, J.-C.; Brittinger, C.; Okada, T.; Mataga, N. *Ber. Bunsenges. Phys. Chem.* **1988**, *92*, 700-706. (d) Sakata, Y.; Nakashima, S.; Goto, Y.; Tatemitsu, H.; Misumi, S.; Asahi, T.; Hagihara, M.; Nishikawa, S.; Okada, T.; Mataga, N. *J. Am. Chem. Soc.* **1989**, *111*, 8979-8981.

(29) (a) Wasieliewski, M. R.; Niemczyk, M. P. *J. Am. Chem. Soc.* **1984**, *106*, 5043-5045. (b) Wasieliewski, M. R.; Niemczyk, M. P.; Svec, W. A.; Pewitt, E. B. *J. Am. Chem. Soc.* **1985**, *107*, 1080-1082. (c) Wasielewski, M. R.; Johnson, D. G.; Svec, W. A.; Kersey, K. M.; Minsek, D. W. *J. Am. Chem. Soc.* **1988**, *110*, 7219-7221.

(30) (a) Moore, T. A.; Gust, D.; Mathis, P.; Mialocq, J.-C.; Chachaty, C.; Bensasson, R. V.; Land, E. J.; Doizi, D.; Liddell, P. A.; Lehman, W. R.; Nemeth, G. A.; Moore, A. L. *Nature (London)* **1984**, *307*, 630-632. (b) Liddell, P. A.; Barrett, D.; Makings, L. R.; Pessiki, P. J.; Gusi, D.; Moore, T. A. *J. Am. Chem. Soc.* **1986**, *108*, 5350-5352. (c) Gust, D.; Moore, T. A.; Moore, A. L.; Barrett, D.; Harding, L. O.; Makings, L. R.; Liddell, P. A.; De Schryver, F. C.; Van der Auweraer, M.; Bensasson, R. V.; Rougee, M. *J. Am. Chem. Soc.* **1988**, *110*, 321-323. See also ref. 16b.

(31) Wasielewski, M. R.; Niemczyk, M. P.; Svec, W. A.; Pewitt, E. B. *J. Am. Chem. Soc.* **1985**, *107*, 5562-5563.

(32) Nishitani, S.; Kurata, N.; Sakata, Y.; Karen, A.; Okada, T.; Misumi, S.; Mataga, N. *J. Am. Chem. Soc.* **1983**, *105*, 7771-7772.

(33) (a) Sakata, Y.; Nishitani, S.; Nishimizu, N.; Misumi, S.; McIntosh, A. R.; Bolton, J. R.; Kanda, Y.; Karen, A.; Okada, T.; Mataga, N. *Tetrahedron Lett.* **1985**, 5207-5210. (b) Osuka, A.; Maruyama, K.; Yamazaki, I.; Tamai, N. *Chem. Phys. Lett.* **1990**, *165*, 392-396.

(34) (a) Cowan, J. A.; Sanders, J. K. M.; Beddard, G. S.; Harrison, R. J. *J. Chem. Soc., Chem. Commun.* **1987**, 55-58. (b) Hunter, C. A.; Meah, M. N.; Sanders, J. K. M. *J. Chem. Soc., Chem. Commun.* **1988**, 692-694. (c) Hunter, C. A.; Meah, M. N.; Sanders, J. K. M. *J. Chem. Soc., Chem. Commun.* **1988**, 694-696. (d) Anderson, H. L.; Hunter, C. A.; Sanders, J. K. M. *J. Chem. Soc., Chem. Commun.* **1989**, 226-227.

(35) (a) Gusi, D.; Moore, T. A.; Moore, A. L.; Makings, L. R.; Seely, G. R.; Ma, X.; Trier, T. T.; Gao, F. *J. Am. Chem. Soc.* **1988**, *110*, 7567-7569. (b) Gust, D.; Moore, T. A.; Moore, A. L.; Seely, G. R.; Liddell, P.; Barrett, D.; Harding, L. O.; Ma, X. C.; Lee, S.-J.; Gao, F. *Tetrahedron* **1989**, *45*, 4867-4892.

(36) (a) Sessler, J. L.; Johnson, M. R.; Lin, T.-Y.; Creager, S. E. *J. Am. Chem. Soc.* **1988**, *110*, 3659-3661. (b) Sessler, J. L.; Johnson, M. R. *Recueil* **1987**, *106*, 222. (c) Sessler, J. L.; Piering, S. *Tetrahedron Lett.* **1987**, 6569-6572. (d) Sessler, J. L.; Johnson, M. R. *Angew. Chem., Int. Ed. Engl.* **1987**, *26*, 678-680. (e) Sessler, J. L.; Johnson, M. R.; Lin, T.-Y. *Tetrahedron* **1989**, *45*, 4767-4784. (f) Sessler, J. L.; Johnson, M. R.; Creager, S. E.; Fettinger, J.; Ibers, J. A.; Rodriguez, J.; Kirmaier, C.; Holten, D. In *Photobiology: The Science and its Applications*; Riklis, E., Ed.; Plenum: New York, in press. (g) Rodriguez, J.; Kirmaier, C.; Sessler, J. L.; Johnson, M. R.; Friesner, R. A.; Holten, D., submitted to *J. Am. Chem. Soc.*

lent itself to the study of possible porphyrin-mediated superexchange.[38] In addition, only one of the model systems reported to date[21b] has been characterized structurally.[39] We thus sought to prepare a series of structurally characterized, energetically defined multicomponent photosynthetic models that would be suitable for the study of long-range photoinduced electron-transfer effects under carefully controlled conditions, and that might allow the question of superexchange to be addressed in well-tailored experiments. In the present paper, we report the synthesis and characterization of several new porphyrin monomers and dimers, including the selectively metalated, quinone-substituted "gable" and "flat" dimers H_2Zn·**10** and H_2Zn·**11** which incorporate the three key biomimetic components: (1) free-base porphyrin photosensitizer, (2) metalloporphyrin intermediate, and (3) quinone acceptor. Elsewhere[36e,f,g] we discuss the results of detailed static fluorescence quenching and transient femtosecond absorption studies carried out with these and related control systems (e.g. H_2Zn·**1**, ZnH_2·**8**, ZnH_2·**10**, ZnH_2·**11**, H_2·**17**, and Zn·**17**) and present evidence for the observation of apparent superexchange-mediated electron transfer in well-defined photosynthetic model systems. Aspects of this work have been communicated earlier.[36a,f]

Results and Discussion

A graphical summary of the newly synthesized porphyrin compounds reported here is given in Figure 1. The free-base forms of these systems were obtained from pyrrolic precursors with use of the general method of Arsenault et al.[40] as modified by Chang and co-workers;[41-43] they were characterized by a variety of means including ^1H NMR, ^{13}C NMR, and UV–visible spectroscopy, mass spectrometry, microanalysis, cyclic voltammetry, and, in the specific cases of H_2·**20** and the bis-copper chelates of **5** and **9**, X-ray diffraction analyses. As appropriate, zinc(II) insertions were then effected from zinc acetate with the selectively monometalated porphyrin dimer complexes H_2Zn·**1**, H_2Zn·**2**, H_2Zn·**3**, H_2Zn·**4**, ZnH_2·**10**, H_2Zn·**10**, ZnH_2·**11**, and H_2Zn·**11** being obtained as the result of regioselective metal binding "titrations".

Scheme II. Synthesis of the Gable Monoquinone H_4·**10**

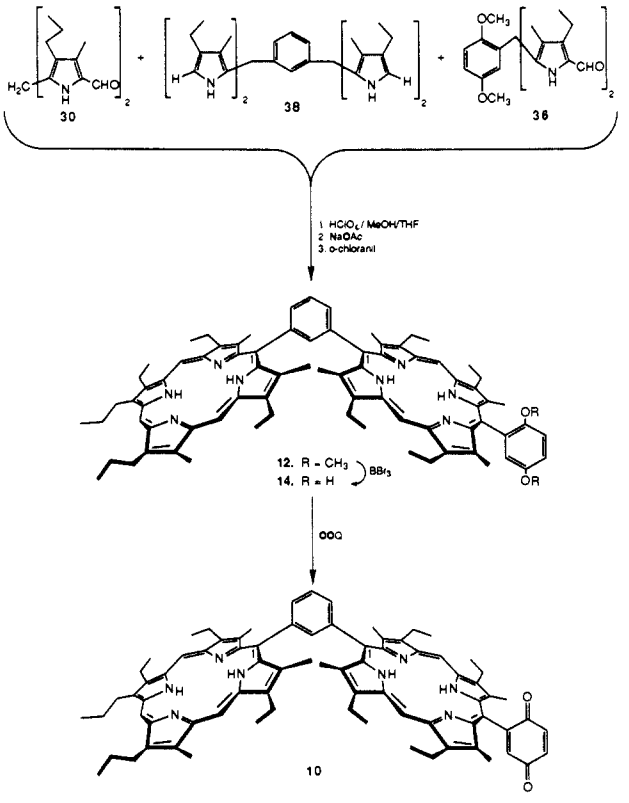

The resulting complexes were characterized by optical and ^1H NMR spectroscopy, as well as, in certain cases, cyclic voltammetric means. Details of this chemistry are discussed in the subsections that follow.

Synthesis of Dipyrromethane Precursors. The synthetic route used to obtain the precursor dipyrromethanes **24–25** is given in Scheme I. Non-phenyl-containing dipyrromethanes **28–33** (Scheme Ia) were made from pyrrolic starting materials (e.g. **25** and **27**) by modifications of literature methods.[44] Since the synthetic transformations involved are straightforward, details of this chemistry are not given in the Experimental Section. They are, however, included in the supplementary material accompanying this paper.

The key starting pyrrole **23** used to prepare precursors **34–45** (vide infra) was made by the general method outlined by Barton and Zard.[45] This elegant new process makes possible the routine preparation of **23** in 100 g batches. Unsubstituted pyrroles such as **23** were previously available only through a more lengthy route.[46] Full details of the new procedure are therefore provided in the Experimental Section.

The acid-catalyzed condensation of **23** with isophthalaldehyde, terephthalaldehyde, benzaldehyde, 2,5-dimethoxybenzaldehyde, or 2,4,6-trimethoxybenzaldehyde in 95% ethanol with an acid catalyst gave dipyrromethane esters **37**, **39**, **41**, **34**, and **43**, respectively, as shown in Scheme I, parts b–d. The control compound **41** and its decarboxylated derivative **42** have been prepared previously.[41] Compounds **37**, **39**, and **41** were isolated directly as powders and subsequently were decarboxylated by heating at reflux in boiling ethylene glycol containing NaOH, to afford **38**, **40**, and **42** in overall yields > 80%. The intermediate esters **34** and **43** did not precipitate but formed glasses or syrups. Con-

(37) A number of acceptor-free oligomeric tetrapyrrolic systems are also known. See for instance: (a) Tabushi, I.; Sasaki, T. *Tetrahedron Lett.* **1982**, *23*, 1913–1916. (b) Tabushi, I.; Sasaki, T. *J. Am. Chem. Soc.* **1983**, *105*, 2901–2902. (c) Tabushi, I.; Kugimiya, S.-I.; Kinnaird, M. G.; Sasaki, T. *J. Am. Chem. Soc.* **1983**, *107*, 4192–4199. (d) Fujita, I.; Netzel, T. L.; Chang, C. K.; Wang, C.-B. *Proc. Natl. Acad. Sci. U.S.A.* **1982**, *79*, 413–417. (e) Netzel, T. L.; Bergkamp, M. A.; Chang, C. K. *J. Am. Chem. Soc.* **1982**, *104*, 1952–1957. (f) Gückel, F.; Schweitzer, D.; Collman, J. P.; Bencosme, S.; Evitt, E.; Sessler, J. *Chem. Phys.* **1984**, *86*, 161–172. (g) Heiler, D.; McLendon, G.; Rogalskyj, P. *J. Am. Chem. Soc.* **1987**, *109*, 604–606. (h) Boxer, S. G.; Bucks, R. S. *J. Am. Chem. Soc.* **1979**, *101*, 1883–1885. (i) Wasielewski, M. R.; Niemczyk, M. P.; Svec, W. A. *Tetrahedron Lett.* **1982**, 3215–3218. (j) Dubowchik, G. M.; Hamilton, A. D. *J. Chem. Soc., Chem. Commun.* **1986**, 665–666. (k) Dubowchik, G. M.; Hamilton, A. D. *J. Chem. Soc., Chem. Commun.* **1986**, 1391–1394. (l) Dubowchik, G. M.; Hamilton, A. D. *J. Chem. Soc., Chem. Commun.* **1987**, 293–295. (m) Osuka, A.; Maruyama, K.; Tomita, H. *Chem. Lett.* **1988**, 1205–1208. (n) Reference deleted in proof. (o) Osuka, A.; Maruyama, K.; Tamai, N.; Yamazaki, I. *J. Chem. Soc., Chem. Comm.* **1988**, 1243–1245. (p) Osuka, A.; Maruyama, K. *J. Am. Chem. Soc.* **1988**, *110*, 4454–4456. (q) Osuka, A.; Ida, K.; Maruyama, K. *Chem. Lett.* **1989**, 741–744. (r) Osuka, A.; Furuta, H.; Maruyama, K. *Chem. Lett.* **1986**, 479–482. (s) Osuka, A.; Maruyama, K. *Chem. Lett.* **1987**, 825–828. (t) Chardon-Noblat, S.; Sauvage, J.-P.; Mathis, P. *Angew. Chem., Int. Ed. Engl.* **1989**, *28*, 593–594. (u) Meier, H.; Kobuke, Y.; Kugimiya, S.-i. *J. Chem. Soc., Chem. Commun.* **1989**, 923–924.

(38) For apparent examples of superexchange electron transfer in non-porphyrin-mediated systems see refs 17h, 18b, 18d, and 30c. See, also: Wasielweski, M. R.; Niemczyk, M. P.; Johnson, D. G.; Svec, W. A.; Minsek, D. W. *Tetrahedron* **1989**, *45*, 4785–4806.

(39) During the course of preparing this manuscript, an X-ray crystal structure of a bis-zinc complex of a phenothroline-linked "gable"-type porphyrin dimer was obtained by Prof. J.-P. Sauvage, Dr. C. Pascard, and coworkers. See: Chardon-Noblat, S. Ph.D. Thesis, Université Louis Pasteur de Strasbourg, 1989.

(40) Arsenault, G. P.; Bullock, E.; MacDonald, S. F. *J. Am. Chem. Soc.* **1960**, *82*, 4384–4396.

(41) Chang, C. K.; Abdalmuhdi, I. *J. Org. Chem.* **1983**, *48*, 5388–5390.

(42) Chang, C. K.; Abdalmuhdi, I. *Angew. Chem., Int. Ed. Engl.* **1984**, *23*, 164–165.

(43) Eaton, S. S.; Eaton, G. R.; Chang, C. K. *J. Am. Chem. Soc.* **1985**, *107*, 3177–3184.

(44) Sessler, J. L.; Hugdahl, J.; Johnson, M. R. *J. Org. Chem.* **1986**, *51*, 2838–2840 and references cited therein.

(45) (a) Barton, D. H. R.; Zard, S. Z. *J. Chem. Soc., Chem. Comm.* **1985**, 1098–1100. (b) Ono, N.; Maruyama, K. *Chem. Lett.* **1988**, 1511–1514. (c) Sessler, J. L.; Mozaffari, A.; Johnson, M. R. *Org. Synth.*, in press.

(46) (a) Archibald, J. L.; Walker, D. M.; Shaw, K. B.; Markovac, A.; MacDonald, S. F. *Can. J. Chem.* **1966**, *44*, 345–362. (b) Franck, B.; Bringmann, G.; Wegner, C.; Spiegel, U. *Justus Liebigs Ann. Chem.* **1980**, 263–274.

sequently these presumed intermediates were not isolated but were saponified and decarboxylated in situ to give **35** and **44** in 97% and 94% overall yields, respectively. When compound **35** was treated with $POCl_3$ in cold DMF, the expected Vilsmier salt did not precipitate even when the temperature was lowered to −20 °C. The solution was therefore poured into water, basified, and treated with methanol to give product **36** in 95% yield. The corresponding aldehyde **45** was obtained in 37% yield from a similar procedure.

Synthesis of Porphyrins. Monomeric porphyrins H_2·**18** and H_2·**21** were prepared by condensation of an α-free dipyrromethane with the appropriate dipyrromethane aldehyde.[40-43] Thus, dialdehyde **36** was condensed with the α-free dipyrromethanes **29** or **42** in methanol with a catalytic amount of perchloric acid, neutralized with NaOAc, and oxidized with *o*-chloranil to yield H_2·**21** and H_2·**18**, respectively, in 40–78% yield. Demethylation of H_2·**21** and H_2·**18** with BBr_3 in dichloromethane at room temperature followed by quenching with methanol and subsequent purification by chromatography on silica gel gave hydroquinones H_2·**22** and H_2·**19**. Subsequent oxidation with 1,2-dichloro-5,6-dicyano-1,4-benzoquinone (DDQ) yielded the quinone-substituted porphyrins H_2·**20** and H_2·**17** in 60–80% yield. The unsubstituted monomeric porphyrin H_2·**16** was made in a similar fashion by condensing equimolar amounts of the α-free dipyrromethane **42** with aldehyde **30** under conditions analogous to those described above.

Bis(quinonylporphyrinyl)benzenes H_4·**3** and H_4·**4**, the synthesis of which has been communicated earlier,[36d] were obtained in a stepwise process analogous to the one used to obtain the phenyl quinone monomer, H_2·**17**. In these procedures, aldehyde **36** was condensed[40-43] with dipyrromethanes **38** or **40** to give dimeric porphyrins H_4·**5** and H_4·**6**, respectively. These were then demethylated with BBr_3 to give the corresponding bis-hydroquinones H_4·**7** and H_4·**8**. Subsequent oxidation with DDQ then gave the bis-quinone dimers H_4·**3** and H_4·**4**.

The pathway to the gable monoquinone dimer, H_4·**10**, is shown in Scheme II. The synthesis of the key precursor, the dimethoxyphenyl-substituted bisporphyrinylbenzene, H_4·**12**, is the same as that described earlier for the gable porphyrin H_4·**1**[44] except that dialdehyde **36** is added to the condensation mixture. Thus, a 1:1:1 mixture of precursors **36**, **30**, and **38** in methanol/THF/1% $HClO_4$ gave after workup roughly equal amounts of the nonsubstituted gable porphyrin H_4·**1**, the monosubstituted system H_4·**12**, and the disubstituted dimer H_4·**5** in an overall yield of 7–9%, along with some monomeric byproducts. The zinc chelates of the porphyrin products were prone to demetalation under the separation conditions (silica gel column, $CCl_4/CHCl_3$ eluent), so the crude reaction mixture was treated instead with copper acetate prior to column chromatography. The resulting copper chelates were much more resistant to demetalation on silica, and, having higher migratory aptitudes than the free-base systems, were easier to purify by column chromatography. Separation of the three main products Cu_2·**1**, Cu_2·**12**, and Cu_2·**5** from each other on silica required a solvent mixture of $CHCl_3$ (12.5%) and CCl_4 (87.5%) rather than pure $CHCl_3$ (which caused Cu_2·**1** and Cu_2·**12** to run together at the solvent front). The copper was removed by treatment with concentrated sulfuric acid, yielding the free base porphyrins H_4·**1**, H_4·**12**, and H_4·**5**, after workup and chromatographic purification. Compound H_4·**12** was then demethylated as before to give H_4·**14** and oxidized with DDQ to give H_4·**10**.

The analogous flat models H_4·**2**, H_4·**13**, and H_4·**6** were prepared by routes similar to those used to obtain H_4·**1**, H_4·**12**, and H_4·**5**. For H_4·**13** and H_4·**6**, the resulting products were then carried on through the hydroquinones H_4·**15** and H_4·**8** to give the quinone-substituted targets H_4·**11** and H_4·**4**. For the flat series, a diformyl butyl-substituted dipyrromethane **33**, rather than a propyl dipyrromethane (i.e. **30**), was used in all but the first series of exploratory porphyrin condensations. This is because the butyl-substituted porphyrins showed better solubility characteristics compared to the propyl-substituted systems and this extra solubility proved crucial in the flat series. The propyl-substituted porphyrins were, however, easier to separate by column chromatography.

Table I. Summary of Bond Distances (Å) and Angles (deg) in H_2·**20**

$N-C_a$ (avg)[a,b]	1.378 (8)	C_a-C_m (avg)	1.393 (12)
C_a-C_b (avg)	1.456 (13)	C_b-C_α (avg)	1.508 (14)
C_b-C_b (avg)	1.364 (5)		
C(20)–C(21)	1.499 (4)		
$N-C_a-C_b$[c]	107.7 (3)–111.3 (3)	$C_a-C_b-C_b$	106.3 (3)–108.3 (3)
$N-C_a-C_m$	122.9 (3)–126.7 (3)	$C_b-C_a-C_m$	122.2 (3)–129.5 (3)
C_a-N-C_a	105.5 (3)–108.8 (2)	$C_a-C_b-C_\alpha$	124.3 (3)–129.5 (3)

[a] The notation "a", and "b", and "m" is that of Hoard, J. L. In *Porphyrins and Metalloporphyrins*; Smith, K. M., Ed.; Elsevier: Amsterdam, 1975; pp 317–380. [b] Here, and elsewhere, the estimated standard deviation given in parentheses is the larger of that calculated for an individual observation on the assumption that the values averaged are from the same population or of that calculated for an individual parameter from the inverse least-squares matrix. [c] Here, and elsewhere, the range of angles of a particular type is listed; in general angles differ significantly and cannot be meaningfully averaged.

Nonetheless, no difficulties were encountered in separating the initial mixtures of Cu_2·**2**, Cu_2·**13**, and Cu_2·**6** obtained from the mixed condensations of **40**, **33**, and **36**.

The flat porphyrin dimer H_4·**9** was obtained by condensation of compounds **40** and **45** in a similar fashion used to obtain flat dimer H_4·**6**. The dicopper chelate Cu_2·**9**, formed in the purification step, gave crystals from chloroform/methanol.

Zinc(II) Complexes. Zinc insertion into the porphyrin monomers H_2·**16**, H_2·**17**, and H_2·**20** was readily performed in the usual way,[47] using zinc acetate in methanol/chloroform, to give Zn·**16**, Zn·**17**, and Zn·**20** in quantitative yield. Similarly, the bis-zinc complexes of all the dimeric porphyrins reported here could be obtained by treating the free-base with excess zinc acetate. This same general approach (using copper acetate) was also used to prepare the bis-copper complexes of dimers **1**, **2**, **5**, **6**, **9**, **12**, and **13** derived from the mixed condensations described above.

The mono zinc complexes of the symmetrical dimers (e.g. ZnH_2·**1**, ZnH_2·**2**, ZnH_2·**3**, and ZnH_2·**4**) were obtained by "titrating" dilute chloroform solutions of the corresponding free-base porphyrin with ca. 1.3 mol equiv of zinc acetate in methanol and purifying by chromatography on silica gel. Similar titrations were also used to prepare the mono-zinc complexes of the unsymmetrical dimers H_4·**10** and H_4·**11**. Here, however, advantage was taken of the differing electronic (and directing) nature of the single substituent available at the quinone and hydroquinone oxidation levels (cf. Scheme III). Specifically, it was found that if the quinones H_4·**10** or H_4·**11** are used for the titration, the zinc preferentially inserts into the unsubstituted porphyrin ring away from ("distal to") the quinone, yielding ZnH_2·**10** and ZnH_2·**11**, respectively. However, if hydroquinones H_4·**14** or H_4·**15** are used instead, the zinc ion preferentially inserts into the nearby (or "proximal") porphyrin ring, yielding H_2Zn·**10** and H_2Zn**11**, respectively, after oxidation and chromatographic purification. Proton NMR analyses were used to establish these regiochemical assignments; these will be discussed shortly.

Characterization. With the exception of the hydroquinone derivatives, all new porphyrins were characterized by ^1H NMR spectroscopy, mass spectrometry, UV–visible spectroscopy, and microanalysis. In many cases, satisfactory ^{13}C NMR spectra were also obtained. Additionally, X-ray structures were obtained for three of the new porphyrins: H_2·**20**, Cu_2·**5**, and Cu_2·**9**. The porphyrin hydroquinones, with the exception of H_4·**14** and H_4·**15**, were not in general characterized, owing to their poor solubility, but instead were directly oxidized to the corresponding quinones. Hydroquinones H_4·**14** and H_4·**15**, however, were used for selective metal insertions and so were characterized by mass spectrometry as well as by ^1H NMR spectroscopy.

Description of the Structure of H_2·20. A summary of bond distances and angles for H_2·**20** is given in Table I. A more complete listing is available in Table SI. The molecular geometry and labeling scheme of the porphyrinic core of the H_2·**20** molecule are shown in Figure 2.

(47) Smith, K. M. *Porphyrins and Metalloporphyrins*; Elsevier: Amsterdam, 1975; pp 884–885.

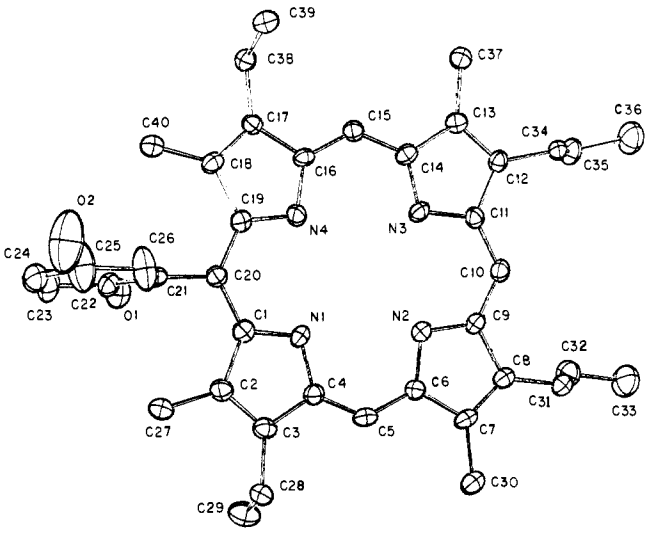

Figure 2. The structure of the H_2·**20** molecule. The labeling scheme is given for the non-hydrogen atoms. Thermal ellipsoids are drawn at the 50% level.

Table II. Summary of Bond Distances (Å) and Angles (deg) for Cu_2·**5**

Cu-N (avg)	2.000 (2)	C_a-C_m	1.389 (19)
N-C_a	1.380 (17)	C_m-C_α	1.512 (10)
C_a-C_b	1.444 (17)	C_b-C_α	1.519 (20)
C_b-C_b	1.341 (20)		
N-Cu-N (cis)	87.0 (2)-93.3 (2)	C_a-N-C_a	104.0 (8)-106.1 (5)
N-Cu-N (trans)	173.3 (2)-177.0 (2)	C_a-C_b-C_b	105.3 (6)-108.2 (7)
Cu-N-C_a	122.4 (4)-130.1 (5)	C_b-C_a-C_m	121.7 (6)-129.7 (6)
N-C_a-C_b	108.4 (7)-112.9 (6)	C_a-C_b-C_α	120.4 (6)-131.7 (6)
N-C_a-C_m	121.1 (6)-126.0 (6)		

The crystal structure of H_2·**20** consists of the packing of discrete monomeric molecules. There are no unusual intermolecular contacts. The plane of the quinone makes an angle of 83.80° with that of the porphyrin. The center-to-center distance between the porphyrin and quinone subunits is 6.48 Å. The porphyrin molecule also contains eight other appendages in addition to the quinone. The four methyl groups, one per pyrrole, lie within ±0.05 Å of their respective pyrrolic planes; the two ethyl groups lie across the porphyrinic plane from each other whereas the two *n*-propyl groups lie on the same side of the molecular plane.

Centroid calculations (CT = center value of the four nitrogen atom positions) indicate that the porphyrin ring is slightly elongated in the C(21)-C(20)-C(10) direction; the two distinct sets of nonbonding interactions involving the centroid (CT) are (in Å): CT-C(1) = 3.164, CT-C(9) = 3.121, CT-C(11) = 3.162, CT-C(19) = 3.141, average = 3.147 Å; CT-C(4) = 3.019, CT-C(6) = 3.015, CT-C(14) = 3.036, CT-C(16) = 2.992, average = 3.016 Å. This deviation is attributable to the different internal porphyrin ring angles at the meso atoms. These angles are found to occur pairwise: C(4)-C(5)-C(6) 130.2(3)° and C(14)-C(15)-C(16) 129.8(3)°, average = 130.0°; C(9)-C(10)-C(11) 125.9(3)° and C(1)-C(20)-C(19) 125.5(3)°, average = 125.7°. There is also a slight ruffling of the porphyrin core, as judged from the best least-squares plane through the 24-atom segment. The mean deviation is 0.076 Å and the maximum deviation is 0.187 (3) Å. The remaining bond distances and angles (Table S1[48]) within the porphyrin are normal in all respects, with internal consistency among chemically equivalent bond parameters.

Description of the Structure of Cu_2·5·(1.5$CHCl_3$)·(0.5CH_3OH). Selected bond distances and angles for the Cu_2·**5**·(1.5$CHCl_3$)·(0.5CH_3OH) molecule are given in Table II. Additional data are in Table SII.[48] The molecular geometry of the Cu_2·**5** molecule is shown in Figure 3. The crystal structure consists of the packing of discrete Cu_2·**5** molecules, 5-fold disordered chloroform molecules, half-occupancy 2-fold disordered chloroform molecules, and half-occupancy methanol molecules; there are no abnormally short interatomic contacts. Bond distances and angles within the Cu_2·**5** molecule are considered normal. The porphyrin cores are both S_4-ruffled. The mean deviation from the best least-squares plane is 0.204 Å for the porphyrin containing atom Cu(1) while it is 0.286 Å for the porphyrin containing atom Cu(2); the maximum displacements are 0.523 (8) Å for atom C(3) and 0.75 (1) Å for atom C(2″) in the two separate porphyrin rings. Distances of interest in relation to biological reaction centers include Cu(1)-Cu(2), 10.49 Å; C(5)-C(5′), 5.01 Å; C(5)-C(41′), 12.38 Å; C(5′)-C(41), 12.91 Å; Cu(1)-CT(1), 6.36 Å; Cu(1)-CT(2), 15.48 Å; Cu(2)-CT(2), 6.33 Å; and Cu(2)-CT(1), 16.01 Å, where CT(1) is the center of the C(41)-C(46) ring and CT(2) is the center of the C(41′)-C(46′) ring. Relevant dihedral angles are given in Table III. Where steric constraints are minimal, e.g. at atoms C(41) and C(41′), the dihedral angles are near the expected 90° (96.3 and 77.8°); at the constrained phenyl bridge these angles are considerably smaller (55.4° and 180-125.0 = 55.0°).

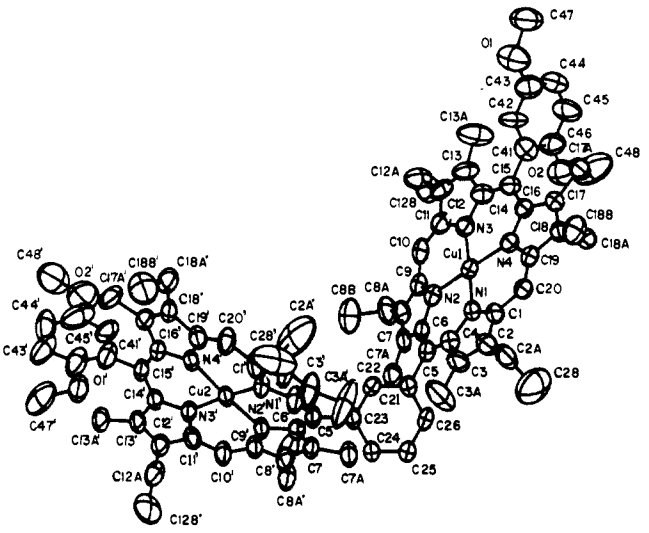

Figure 3. The structure of the Cu_2·**5** molecule. The hydrogen atoms are omitted. The 50% thermal ellipsoids are shown.

Table III. Dihedral Angles (deg) in the Copper Dimers

	Cu_2·**5**	Cu_2·**9**
Ph1-Por1[a]	96.3	93.8
Ph1-Br	41.0	164.6
Ph1-Por2	119.8	93.8
Ph1-Ph2	66.6	0
Por1-Br	55.4	101.6
Por1-Por2	105.9	0.0
Por1-Ph2	59.9	93.8
Br-Por2	125.0	101.6
Br-Ph2	47.5	164.6
Por2-Ph2	77.8	93.8

[a] The dimers are "strung" together in the order Ph1-Por1-Br-Por2-Ph2, where Ph = terminal phenyl ring, Por = porphyrin group, and Br = phenyl bridge.

Figure 3 also shows that both dimethoxy linkages have their orientations such that the methoxy linkage on the interior of each porphyrin unit adopts the sterically least encumbered position. Thus, the two porphyrin subunits and their substituents help define what can be considered an overall "skewed" arrangement contained within the context of a general gable-type configuration. The obvious structural similarity between this completely synthetic system and parts of the reaction center (notably the Bchl and Bph pair) is a feature we consider to be of particular interest.

Description of the Structure of Cu_2·9·(2$CHCl_3$). The crystal structure of Cu_2·**9**·(2$CHCl_3$) consists of the packing of one centrosymmetric Cu_2·**9** molecule and two chloroform molecules in

(48) Supplementary material.

Scheme III. Synthesis of Monometalated Gable and Flat Monoquinones, H_2Zn·**10**, ZnH_2·**10**, H_2Zn·**11**, and ZnH_2·**11**

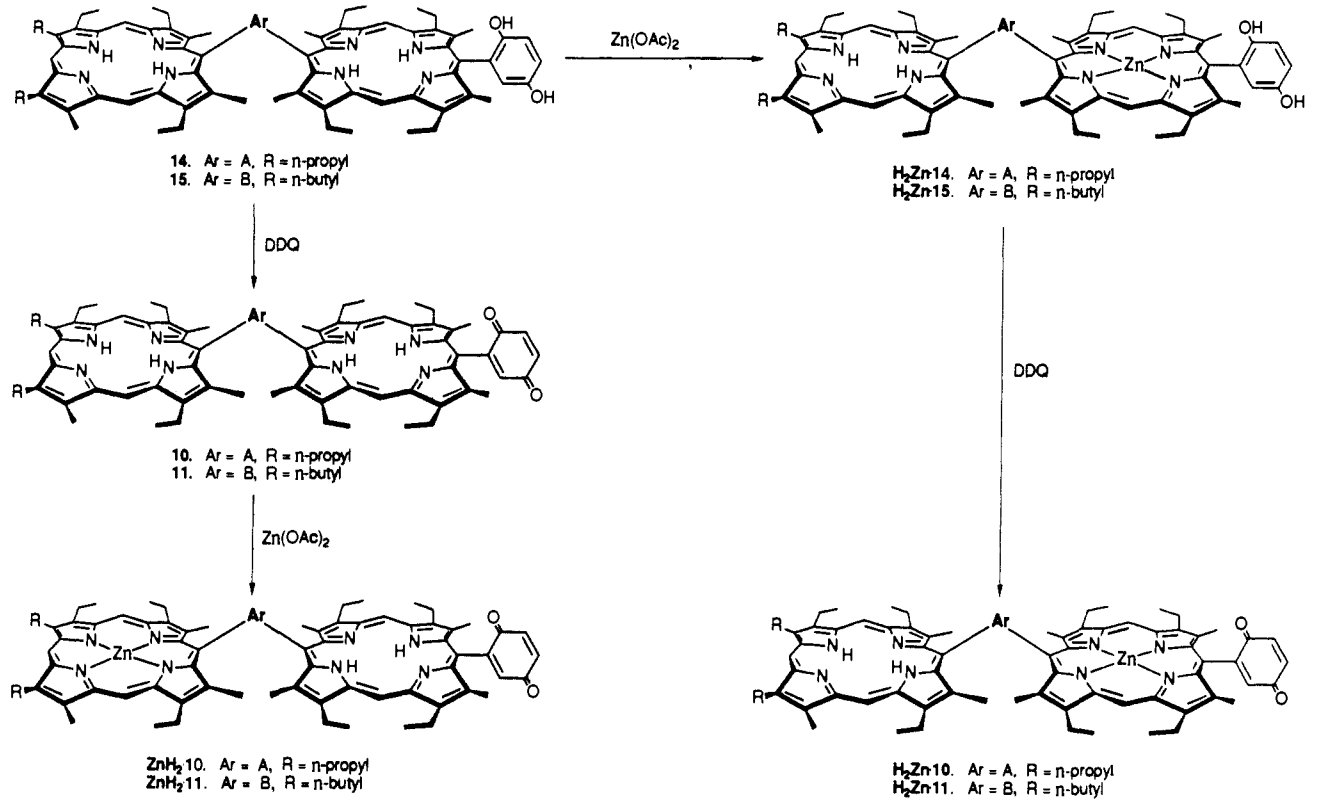

the unit cell. There are no unusual intermolecular contacts. A drawing of the molecule is given in Figure 4. Selected bond distances and angles for the Cu_2·**9** molecule are given in Table IV. Additional data are given in Table SIII.[48] Bond distances and angles are normal. As in the other structures reported here the porphyrin core in Cu_2·**9** is S_4-ruffled; the mean deviation from the best least-squares plane is 0.129 Å and the maximum deviations from this plane are 0.372 (5) Å for atom C(5) and −0.273 (5) Å for atom C(10). Two of the ethyl linkages on the porphyrin ring are "up" while the other two are "down". All appendages (both ethyl and methoxy) are ordered in this structure, as is the chloroform of solvation.

Distances of interest in relation to biological reaction centers include Cu(1)–Cu(2), 12.77 Å; C(5)–C(5′), 5.86 Å; C(5)–C(24′), 14.03 Å; Cu–CT, 6.33 Å; and Cu–CT′, 18.82 Å. As is obvious from a comparison of Figures 3 and 4, the Cu_2·**9** molecule, with its 1,4-attachment of porphyrin groups to the bridging phenyl ring, is considerably more extended than is the Cu_2·**5** molecule, with its 1,3-attachment of porphyrin groups. The Cu_2·**9** molecule is also less sterically constrained, as the dihedral angles of Table III indicate. Note that these dihedral angles are near to 0°, 90°, or 180° so that successive rings are nearly perpendicular to each other.

Proton NMR Spectra. All pyrrolic precursors gave satisfactory ^{1}H NMR spectra, except for the butyl dipyrromethanes **31**–**33**, for which a poorly resolved butyl substituent fine structure was observed. The reason for this lack of resolution is unknown; however compounds **31**–**33** had sharp melting points and appropriate mass spectra and are considered to be pure. As noted earlier, all the porphyrins except the hydroquinones gave satisfactory proton NMR spectra in $CDCl_3$ at 300 or 360 MHz. For the hydroquinones, low solubility hampered accurate analyses. For the important specific cases of H_4·**14** and H_4·**15** (the precursors to H_2Zn·**10** and H_2Zn·**11**), where ^{1}H NMR spectral characterizations were deemed essential, methanol-d_4 was added to the NMR tubes to increase solubility. As a result, the internal pyrrole regions of these porphyrins were not observed, owing to rapid tautomeric exchange.

The proton NMR spectrum of the monoquinone gable porphyrin H_4·**10** (Figure 5) is illustrative of those obtained for the 1,3-phenyl-linked systems. It, and the spectra of other compounds in the gable series, is characterized by two sets of phenyl-type ring absorbances corresponding to the bridging phenyl ring protons, appearing as a set of resonances from 7.95 to 8.95 ppm, and the quinone ring protons, which are observed as a tightly clustered series of peaks centered at roughly 7.3 ppm. Importantly, the first of these appears as a progression of singlet-, triplet-, and doublet-type signals, as would be expected for the proposed 1,3-phenyl-linked structure. Also consistent with the proposed structure is the observation of three different types of meso-H signals in the general range of 9.8 to 10.15 ppm. These signals, which integrate in the ratio 2:2:1, appear to be diagnostic of transannular monosubstituted meso-linked porphyrin dimers and

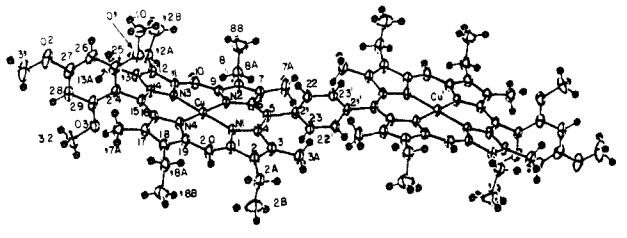

Figure 4. The structure of the Cu_2·**9** molecule. The non-hydrogen atoms are labeled. For the non-hydrogen atoms the 50% probability ellipsoids are shown. The hydrogen atoms are drawn artificially small for the sake of clarity.

Table IV. Summary of Bond Distances (Å) and Angles (deg) for Cu_2·**9**

Cu–N (avg)	2.003 (6)	C_a–C_m	1.389 (9)
N–C_a	1.378 (16)	C_b–C_α	1.496 (13)
C_a–C_b	1.446 (16)	C_α–C_β	1.507 (15)
C_b–C_b	1.356 (8)		
N–Cu–N (cis)	86.6 (1)–93.1 (2)	C_a–N–C_a	105.0 (3)–106.0 (4)
N–Cu–N (trans)	178.2 (2)–179.1 (2)	C_a–C_b–C_b	105.4 (4)–107.8 (4)
Cu–N–C_a	123.8 (3)–130.9 (3)	C_b–C_a–C_m	122.6 (4)–128.3 (4)
N–C_a–C_b	108.0 (4)–112.6 (4)	C_a–C_b–C_α	124.5 (4)–129.9 (4)
N–C_a–C_m	122.8 (4)–125.6 (4)		

Table V. Crystal Data and Data Collection

compound	H_2·**20**	Cu_2·**5**·1.5$CHCl_3$·0.5MeOH	Cu_2·**9**·2$CHCl_3$
formula	$C_{40}H_{44}N_4O_2$	$C_{88}H_{93.5}Cl_{4.5}Cu_2N_8O_{4.5}$	$C_{90}H_{96}Cl_6Cu_2N_8O_6$
formula weight	612.82	1621.91	1725.63
space group	$C_{2h}^5 - P2_1/c$	$C_i^1 - P\bar{1}$	$C_i^1 - P\bar{1}$
a, Å	8.241 (6)	19.015 (4)	12.036 (3)
b, Å	30.34 (3)	19.043 (6)	12.762 (3)
c, Å	13.502 (12)	12.957 (5)	14.353 (3)
α, deg	90	109.90 (2)	94.64 (1)
β, deg	92.86 (1)	108.84 (2)	103.54 (1)
γ, deg	90	101.86 (2)	104.68 (1)
V, Å^3	3375	3904	2050
t, °C	−162	−162	−115
Z	4	2	1
ρ_{calc}, g/cm^3	1.207	1.379	1.397
crystal vol, mm^3	0.0068	0.0149	0.0041
radiation, Å	Mo Kα ($\lambda(\alpha_1)$ = 0.7093) graphite monochromator)	Cu Kα ($\lambda(\alpha_1)$ = 1.54056) (β filter)	Cu Kα ($\lambda(\alpha_1)$ = 1.54056) (β filter)
μ, cm^{-1}	5.51	25.56	29.34
transmission factors	–	0.510–0.661	0.614–0.878
scan type	ω	$\omega - 2\theta$	$\omega - 2\theta$
scan range, deg	±0.7(ω)	±0.8(ω)	±0.85(ω)
scan speed, deg/min	2.0(ω); rescan ≤ 100 s	4.0(ω); rescan ≤ 40 s	3.2(ω); rescan ≤ 50 s
λ^{-1} sin θ range, Å$^-$	0.0615–0.5958	0.023–0.562	0.023–0.627
data collected	$h, k, \pm l$	$\pm h, \pm k, l$	$\pm h, \pm k, l$
unique data	5894	11574	8318
unique data ($F_o^2 > 3\sigma(F_o^2)$)	3307	6909	4534
no. of variables	434	1015	505
$R(F_o^2)$	0.101	0.130	0.105
$R_w(F_o^2)$	0.161	0.194	0.152
$R(F_o)$ ($F_o^2 > 3\sigma(F_o^2)$)	0.069	0.085	0.067
error observation of unit weight	1.44	1.84	1.44

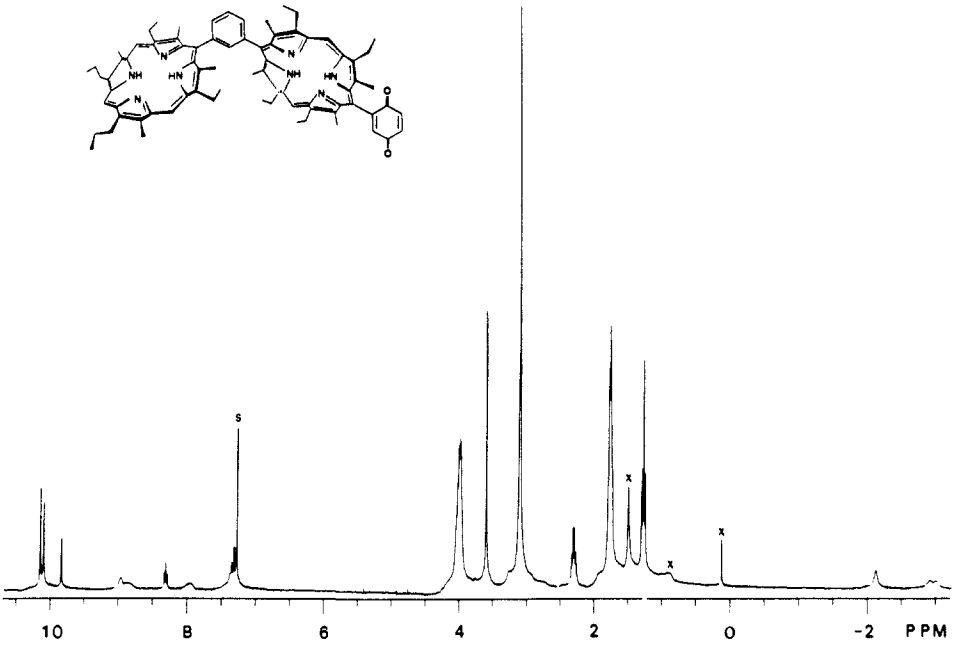

Figure 5. Proton NMR spectrum of H_4·**10** in $CDCl_3$ at 300 MHz. The designations s and x denote solvent and impurity peaks, respectively.

were also observed for compounds H_4·**11**–H_4·**15**. As expected, however, they were not observed in the symmetrical systems H_4·**1** and H_4·**2** (which showed a 2:1 ratio of singlets in the meso region), or in H_4·**3**–H_4·**8** (which displayed simple singlets). A further diagnostic feature of H_4·**10**, and the other unsymmetrical systems reported here (i.e. H_4·**11**–H_4·**15**), is the well-separated set of two distinct N–H signals observed in the internal pyrrole portion of the ^{1}H NMR spectrum (Figure 5). These two sets of peaks, which in the specific case of H_4·**10** resonate at δ = −2.1 and −3.0 ppm, are indicative of the different electronic environments extant for the two different porphyrin subunits. Such distinct pairs of signals are observed neither in the unsubstituted dimers H_4·**1** and H_4·**2** nor in the symmetrically substituted systems H_4·**3**–H_4·**8**. These two classes of compounds each display only a single set of pyrrolic N–H resonances, at roughly −3.0 and −2.1 ppm, respectively. Thus, the higher field pyrrole N–H signals observed in H_4·**10**–H_4·**15** may readily be assigned to the *unsubstituted* porphyrin, and those at lower field to the *substituted* subunit. Interestingly, in all cases studied, the signal at higher field was always found to be split into a fairly well-resolved pair at room temperature, suggesting that complete N–H tautomerization is slow on the NMR time scale. This phenomenon is apparently a general feature of the substitution pattern and does not derive from some special effect associated with the monosubstituted 1,3-phenyl- or 1,4-phenyl-linked dimeric configurations: Almost identical chemical shifts and splitting patterns were observed for the pyrrole

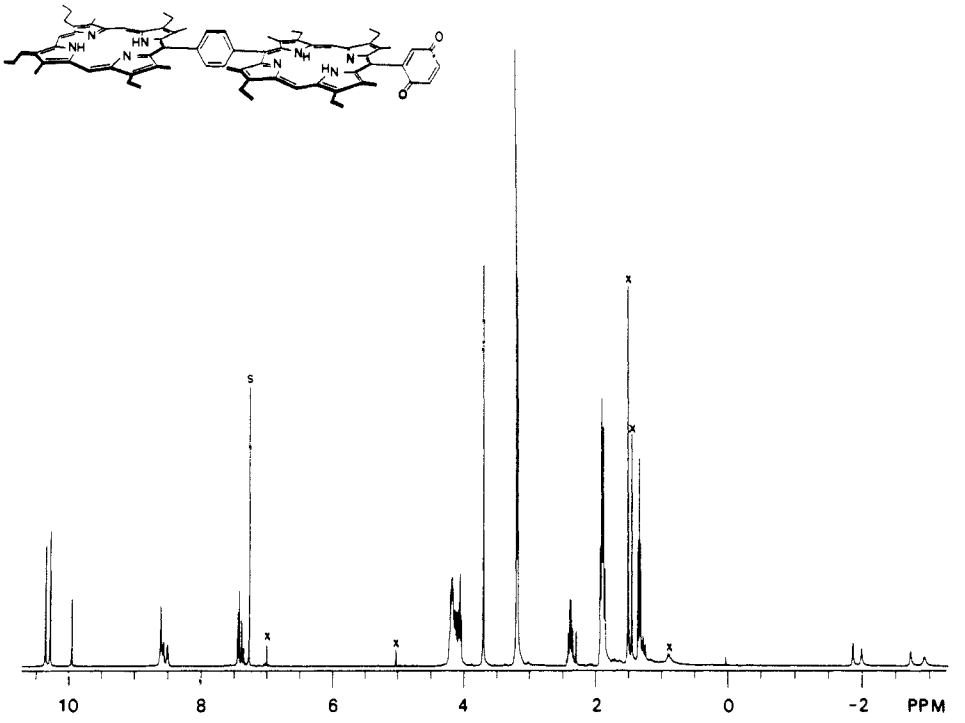

Figure 6. Proton NMR spectrum of H_4·**11** in $CDCl_3$ at 300 MHz. The designations s and x denote solvent and impurity peaks, respectively.

N–H protons of monomers H_2·**16**, H_2·**20**, H_2·**21**, and H_2·**22**. By contrast, the pyrrole N–H signals observed for the disubstituted subunits of dimers H_4·**10**–H_4·**15** always appeared as broad singlets, as did those for the reference dimers H_4·**3**–H_4·**8** and control monomers H_2·**17**–H_2·**19**.

The ^{1}H NMR spectrum of the monoquinone porphyrin dimer H_4·**11** (Figure 6) is typical of those observed for the flat series of 1,4-phenyl-linked dimers. As expected, the spectra of these two species are similar in the aliphatic (1.0–4.0 ppm), meso (9.8–11 ppm), and internal N–H (−2 to −3 ppm) regions because of the similarity of their overall substitution patterns. The resonances of the bridging phenyl protons in the 8–9 ppm region are different for the flat and gable dimers, as expected from their different (1,3 vs 1,4) ring placement. Unexpectedly, however, the flat dimers H_4·**2**, H_4·**4**, H_4·**6**, H_4·**9**, H_4·**11**, H_4·**13**, and H_4·**15** show marked differences *between each other* in the bridging phenyl region: Compounds H_4·**2** and H_4·**9** display sharp singlets (no splitting) in this region, H_4·**4** and H_4·**6** show symmetric splitting patterns, and H_4·**11**, H_4·**13**, and H_4·**15** show asymmetric splittings. Since the main differences between all these compounds are in the transverse meso substituents, this complexity implies that differences in the transverse meso substituents can and do affect the magnetic environment of the central phenyl protons even though they are some 10 Å away. The bridging phenyl resonances of H_4·**4** and H_4·**6** are most useful for discussion (Figures 7 and 8). At 23 °C, the bridging phenyl resonance of the flat bisquinone H_4·**4** ($CDCl_3$) consists of two singlets around a doubled doublet, centered at 8.57 ppm (total width = 75 Hz). The coupling constant for the doubled doublet in H_4·**4** is 8 Hz, and tertiary splitting (<1 Hz) is clearly visible at temperatures below 20 °C. The bridging phenyl region of H_4·**6** (toluene-d_8 or $CDCl_3$), whose features are similar to but less sharp than that of H_4·**4**, is centered at 8.19 ppm (total width = 35 Hz). The coupling constant for the doubled doublet of H_4·**6** is 7–8 Hz.[49] We believe the origins of these splitting effects arise from the differing placement of the ortho substituents on the transverse meso groups, as shown for H_4·**4** in Figure 9. The ortho atoms on the meso-phenyl groups of the porphyrin rings could cause the electron distribution on opposite faces of the porphyrin ring to be disymmetric with respect

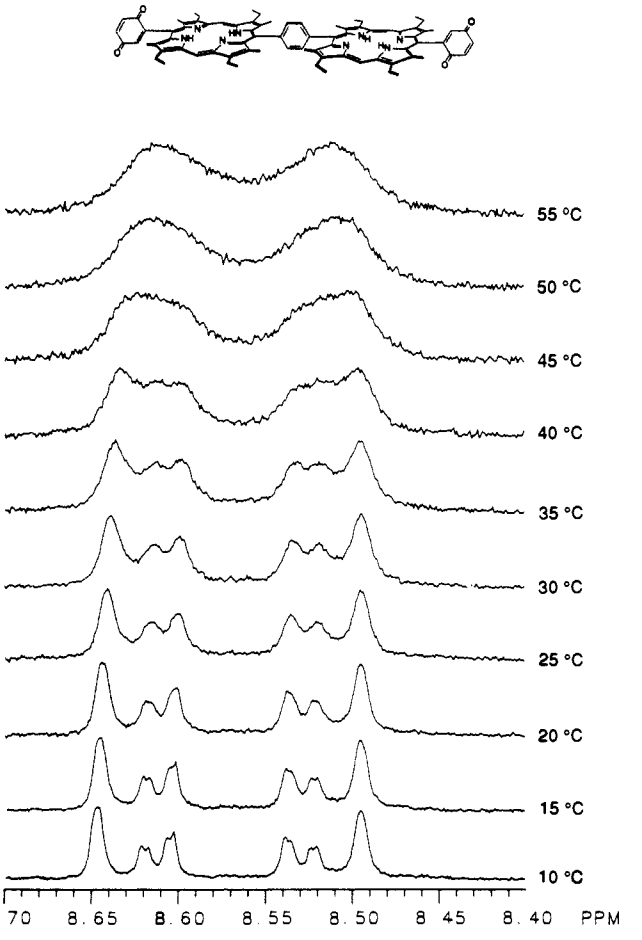

Figure 7. Proton NMR ($CDCl_3$) of the bridging phenyl resonances of H_4·**4** recorded at 500 MHz.

to the plane of the ring, thus creating different magnetic environments for the adjacent phenyl protons on opposite faces of the porphyrin ring. We believe this occurs for the bridging phenyl protons of compounds H_4·**4** and H_4·**6**. To our knowledge, splitting effects from conformational differences between such well-sepa-

(49) The observed coupling constant of 7–8 Hz for both H_4·**4** and H_4·**6** is consistent with ortho splitting in a benzene ring: Rahman, A. *Nuclear Magnetic Resonance: Basic Principles*; Springer-Verlag: New York, 1986.

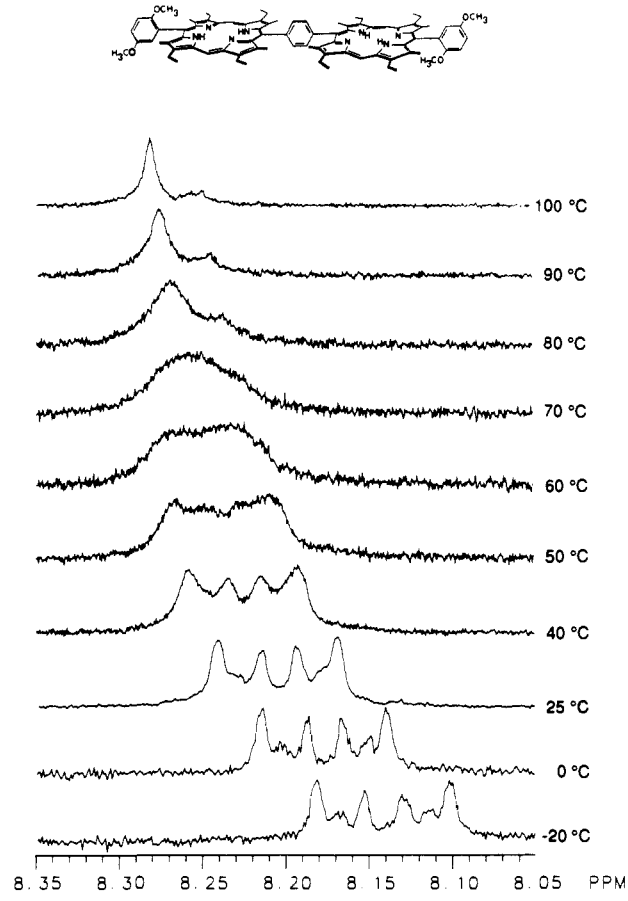

Figure 8. Proton NMR (toluene-d_8) of the bridging phenyl resonances of H_4·**6** recorded at 500 MHz.

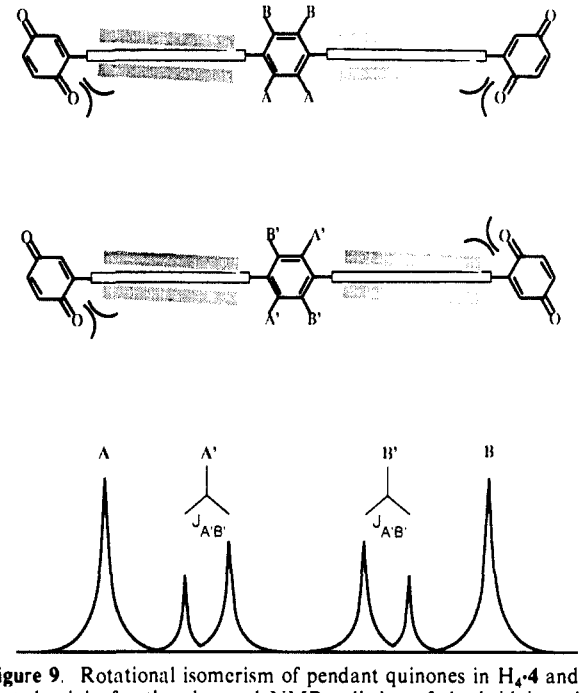

Figure 9. Rotational isomerism of pendant quinones in H_4·**4** and suggested origin for the observed NMR splitting of the bridging phenyl region of compounds H_4·**4** and H_4·**6**.

rated atoms in a molecule are unprecedented. Porphyrin rings, however, are well known for having strong ring currents, and it is conceivable that a steric perturbation on one face of a porphyrin ring can affect the electronic distribution around both faces of that ring. As shown in Figure 9, compound H_4·**4** may consist of syn- (C_{2h} symmetry) and anti- (C_{2v} symmetry) rotational atropisomers ("rotamers"). In the anti rotamer, the bridging phenyl protons ortho to each other are magnetically identical and hence do not split each other; a pair of singlets results. By contrast, in the syn rotamer, the ortho protons are in different magnetic environments, so they split each other, and a doubled doublet results. This pattern, modeled at the bottom of Figure 9, accounts well for the observed splitting in Figures 7 and 8. Here, however, it is important to note that the particular proton assignments are arbitrary: We are currently unsure as to whether, in fact, it is the "A" protons which lie upfield as illustrated or whether it is the "B" protons; experiments are in progress to resolve this and other issues associated with these unusual splitting effects.

Variable-temperature studies of the bridging phenyl resonances of H_4·**4** and H_4·**6** are noteworthy (Figures 7 and 8). When the samples are warmed, both H_4·**4** and H_4·**6** show bridging phenyl fine structure coalescence in the range of 40 to 50 °C. This indicates that the A and B protons in Figure 9 are undergoing exchange. This coalescence process may involve thermally activated rotation of one or more of the three bridging phenyl or pendant phenyl/quinone groups on or between the porphyrin rings of H_4·**4** and H_4·**6**. Rotation of the outermost, or pendant, substituents would serve to equilibrate the C_{2v} and C_{2h} rotamers and hence to scramble completely the A and B bridging phenyl protons. By contrast, rotation of only the bridging phenyl subunit would serve to scramble only the A and B phenyl protons within each still chemically distinct C_{2v} and C_{2h} diasteriomeric set. Here, however, even in the absence of further pendant phenyl or quinone rotations, complete apparent coalescence would still be observed if the chemical shifts of the now-unsplit central phenyl protons happen to be identical for each (C_{2v} and C_{2h}) rotameric system.

Quantitative studies, carried out with use of the GENXCH program (cf. Experimental Section), indicate that the barriers for the exchange in H_4·**4** and H_4·**6** are about 18 and 15 kcal/mol, respectively. These values are somewhat smaller than those for rotational isomerizations involving ortho-substituted phenylporphyrins,[50-52] for which barriers as high as 26 kcal/mol have been found (in, for instance, 5,15-bis(*o*-aminophenyl)-2,8,12,18-tetraethyl-3,7,13,17-tetramethylporphine[50]), and are much more in line with those expected for simple unsubstituted or para-substituted tetraphenylporphyrin atropisomerization processes.[53] The observed coalescence thus probably involves rotations of the internal, unsubstituted phenyl subunit (only) and not the outer ortho-substituted appendages. Over the temperature range studied we would not expect to see manifestations of rotations of these outer appendages because the barriers should be on the order of 25 kcal/mol.[50]

Selective Monometalation. A second important use of ^{1}H NMR spectroscopy was to determine the regiochemistry of the selective monometalations shown in Scheme III. Evidence for the regiochemical assignments in the gable series is given in Figure 10, which shows the internal pyrrole region of several different monometalated porphyrins: H_4·**10**, ZnH_2·**10**, H_2Zn·**10**, ZnH_2·**1**, and ZnH_2·**3**. Compound H_4·**10** shows two internal pyrrole resonances, at ca. −2 and −3 ppm. By contrast, ZnH_2·**10** shows only a resonance at −2 ppm, and H_2Zn·**10** shows only a resonance at −3 ppm (plus a trace of the nonmetalated H_4·**10**). Compound ZnH_2·**1** has a resonance only at −3 ppm and ZnH_2·**3** has a resonance only at −2 ppm. This implies that ZnH_2·**10** has internal pyrrole protons only in the proximal, quinone-substituted ring and H_2Zn·**10** has internal pyrrole protons only in the distal, unsubstituted ring. A similar result was obtained for the flat monoquinone porphyrins ZnH_2·**11** and H_2Zn·**11**, which were prepared in an analogous fashion as described above.

Carbon NMR Spectra. Satisfactory ^{13}C NMR spectra were obtained for all the porphyrins reported here, with the exception of the hydroquinones H_4·**7**, H_4·**8**, H_4·**14**, H_4·**15**, H_2·**19**, and H_2·**22**, and the flat dimer H_4·**9**, all of which proved too insoluble for such

(50) Young, R.; Chang, C. K. *J. Am. Chem. Soc.* **1985**, *107*, 898-909.
(51) Walker, F. A. *Tetrahedron Lett.* **1971**, 4949-4952.
(52) Gottwald, L. K.; Ullman, E. F. *Tetrahedron Lett.* **1969**, 3071-3074.
(53) (a) Eaton, S. S.; Eaton, G. R. *J. Am. Chem. Soc.* **1977**, *99*, 6594-6599. (b) Eaton, S. S.; Eaton, G. R. *J. Am. Chem. Soc.* **1975**, *97*, 3660-3666.

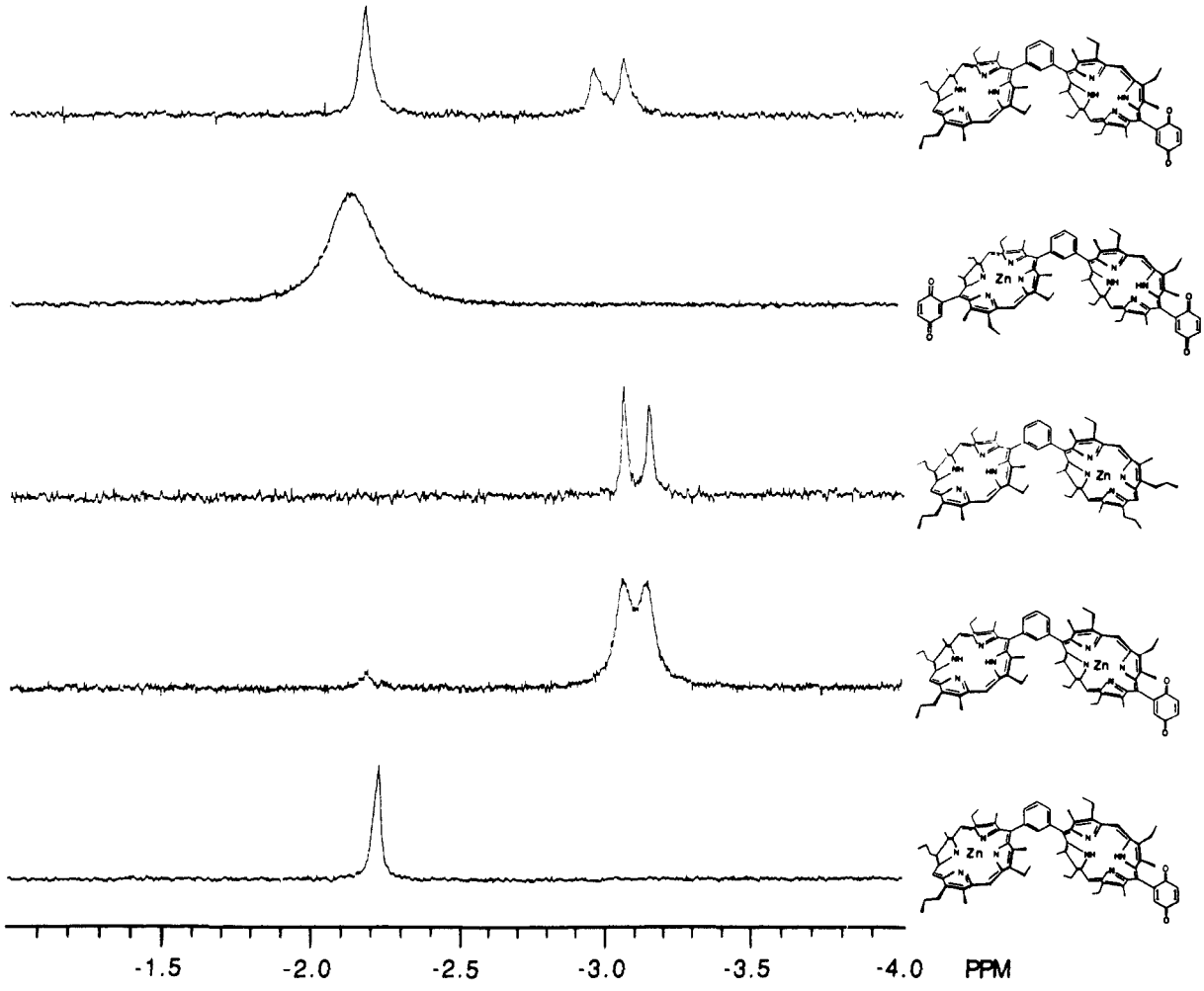

Figure 10. Proton NMR ($CDCl_3$) of internal pyrrole region at 300 MHz for (top to bottom) H_4·**10**, ZnH_2·**3**, ZnH_2·**1**, H_2Zn·**10**, and ZnH_2·**10**.

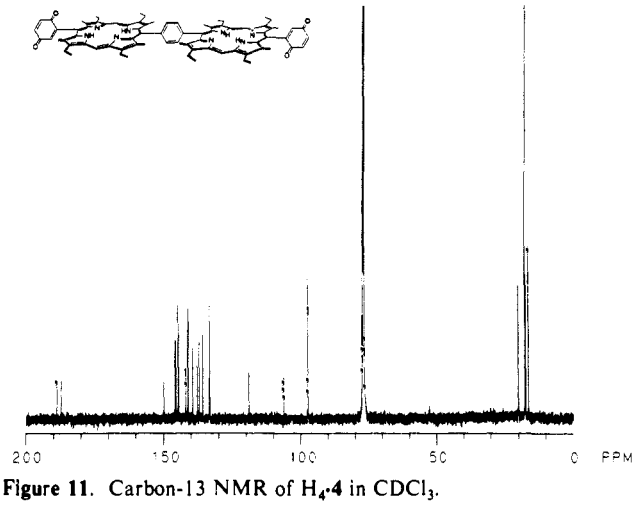

Figure 11. Carbon-13 NMR of H_4·**4** in $CDCl_3$.

analyses. A sample spectrum, that of the flat bisquinone dimer H_4·**4**, is shown in Figure 11. Peak assignments were not made for the aromatic region, because of the complexity of the spectra (owing presumably to the asymmetric nature of the porphyrin dimers), but were found to correlate well with the expected structures in the aliphatic (0–50 ppm) region. Carbon NMR studies were primarily used to establish the presence of the quinone moiety in the molecule. The carbon atoms of the carbonyl group associated with this subunit were found to resonate at 187–189 ppm. Since these quinone NMR resonances appear far downfield from those of any other carbon nuclei present in the molecules and are not found in the quinone-free precursors, this ^{13}C NMR test provided an unambiguous indication of the presence of a quinone group in the sample.

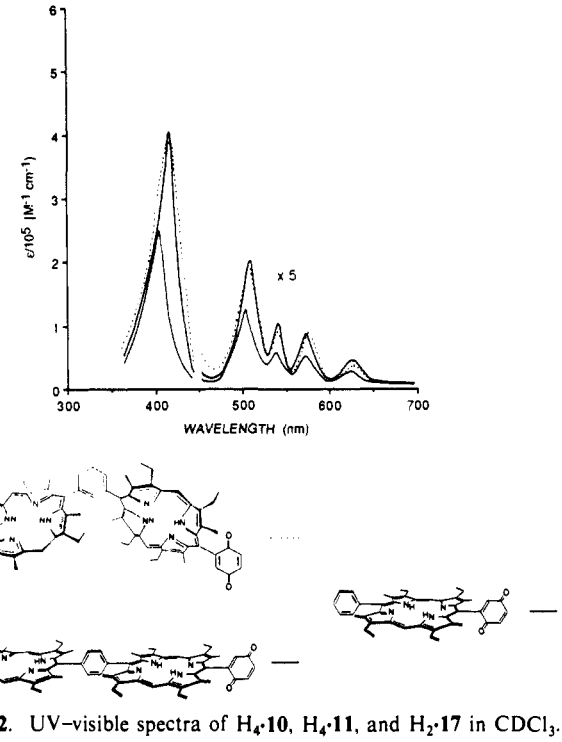

Figure 12. UV-visible spectra of H_4·**10**, H_4·**11**, and H_2·**17** in $CDCl_3$.

UV-Visible Spectra. UV-visible spectra of some of the compounds synthesized are shown in Figures 12–14.[54] Complete

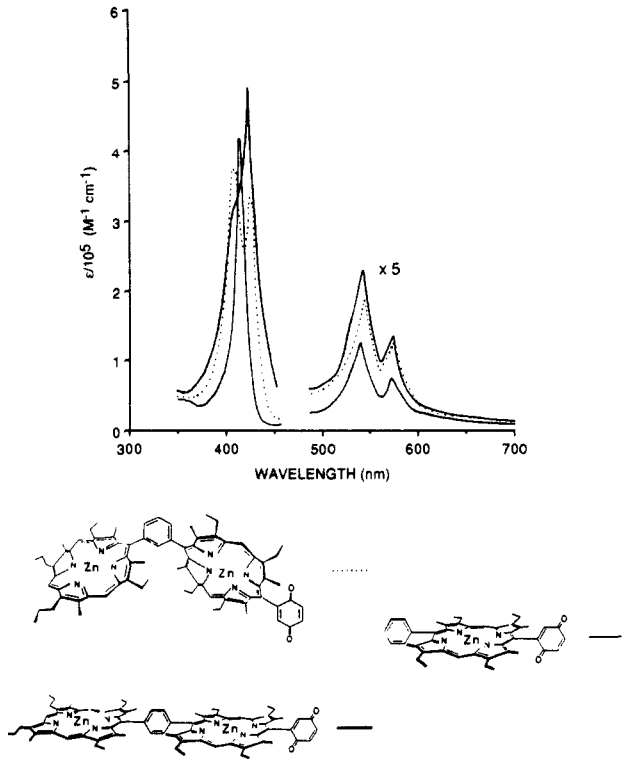

Figure 13. UV–visible spectra of Zn_2·**10**, Zn_2·**11**, and Zn·**17** in $CDCl_3$.

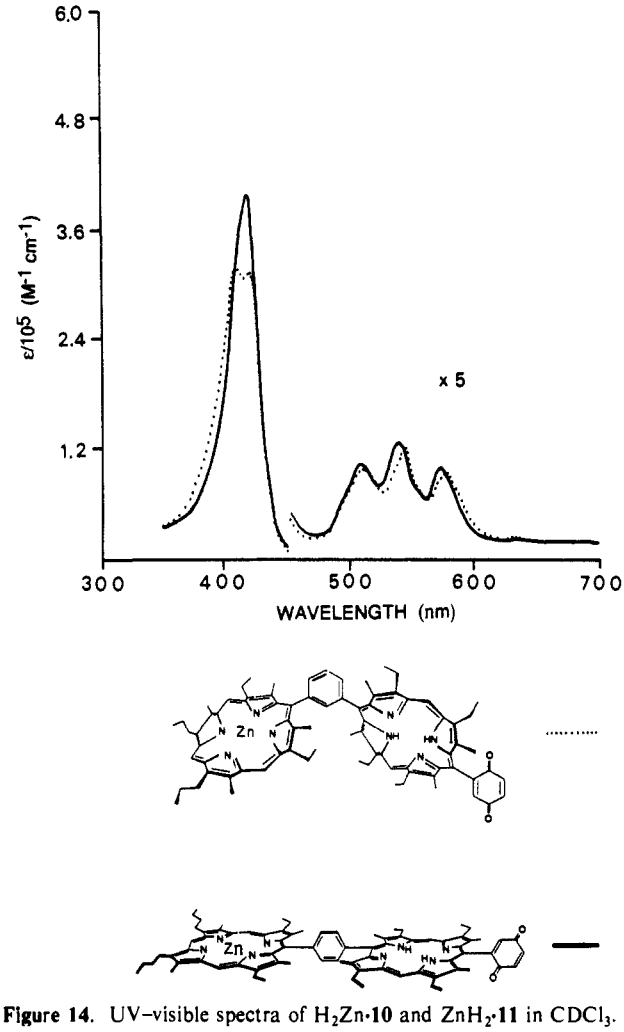

Figure 14. UV–visible spectra of H_2Zn·**10** and ZnH_2·**11** in $CDCl_3$.

UV–visible data for the other porphyrins are given in the Experimental Section. Repeated measurements gave 5–10% variance in the extinction coefficients; the wavelength values (λ_{max}) are considered to be accurate to within 1 nm.

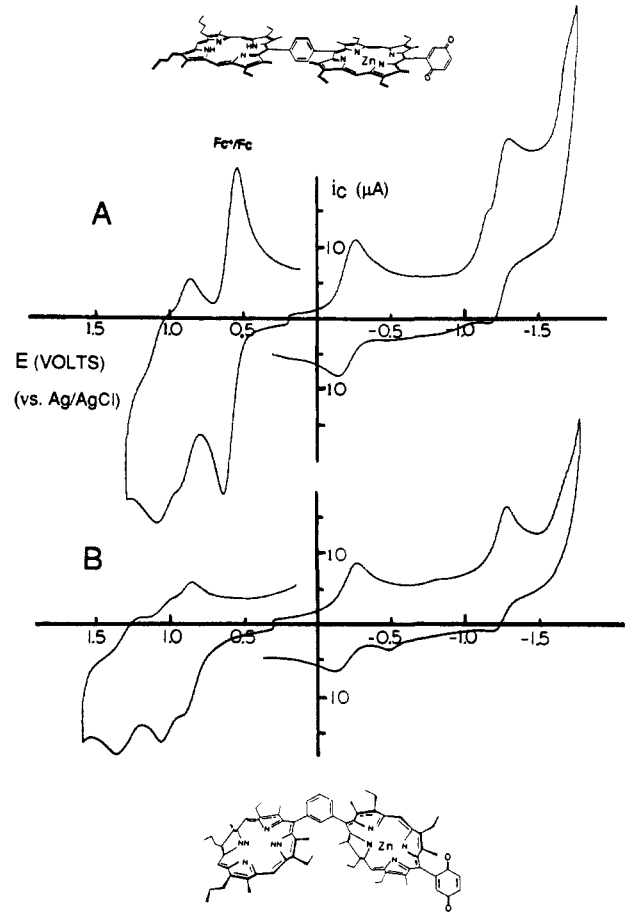

Figure 15. Cyclovoltammograms (CH_2Cl_2) of H_2Zn·**10** and H_2Zn·**11**. Fc/Fc^+ denotes ferrocene/ferrocinium reference.

Figure 12 shows the absorbances of the free base dimers H_4·**10** and H_4·**11** as well as the monomer H_2·**17**. Compounds H_4·**10** and H_4·**11** show approximately the same extinction coefficient in the Soret region, as well as in the visible or "Q" band region. The differences between the UV–visible absorbances of compounds H_4·**10**, H_4·**11**, and H_2·**17** become more pronounced upon complexation of these compounds with zinc (Figure 13). The order of molar absorptivity again is Zn_2·**11** > Zn_2·**10** > Zn·**17**. Excitonic interactions between the porphyrin rings in Zn_2·**10** result in the "split Soret" band typical of 1,3-phenyl-linked, bis-porphyrinylbenzenes,[37a-c,q,44] with two peaks at 407 and 424 nm. The flat dimer Zn_2·**11** also shows some excitonic interaction: Only a slight shoulder at 412 nm is seen, with the major peak appearing at 424 nm. Figure 14 shows the UV–visible spectra of the monometalated gable and flat monoquinones ZnH_2·**10** and ZnH_2·**11**. Again, evidence for excitonic interactions is observed in the Soret region (as manifest by spectral shifts and/or splittings) but to a much lesser extent than in the corresponding bis-zinc derivatives, Zn_2·**10** and Zn_2·**11**. A more detailed analysis of the dipole coupling parameters for various gable and flat dimers has been performed and is reported elsewhere.[55]

Electrochemistry. The results of a systematic survey of model compounds H_4·**1**, H_4·**2**, H_4·**10**, H_4·**11**, H_2·**16**, H_2·**17**, and their zinc chelates is presented in Table VI, and two sample voltammograms are shown in Figure 15.

a. Monomers. In the quinone-free systems, the redox potentials for both oxidation and reduction (in dichloromethane) of the

(54) The spectra in Figures 12 and 13 have been published previously.[36e] However, an error in draftmanship led these figures to be plotted in such a way that the wavelength (x axis) ended up in both cases being displaced incorrectly by roughly 50 nm.

(55) Won, Y.; Friesner, R. A.; Johnson, M. R.; Sessler, J. L. *Photosynth. Res.* **1989**, *22*, 201–210.

Table VI. Electrochemical Data (in CH_2Cl_2) for Selected Porphyrins Prepared in this Study[a]

compd	O_2	O_1	Q_1	Q_2	R_1	R_2	$\Delta E_{R/O}$	note
H_4·**1**		0.39[c]			−1.80		2.19	
		0.53[c,f]			−1.90[f]			
ZnH_2·**1**	0.46[c]	0.22			−1.79		2.01	
Zn_2·**1**		0.19			−2.02		2.21	*d*
		0.35[f]						
H_4·**2**	0.77[c]	0.46[c]			−1.75		2.21	
ZnH_2·**2**	0.50[c]	0.35			−1.83		2.18	*d*
Zn_2·**2**		0.30			−1.95		2.25	*d*
H_4·**10**		0.43[c]	−0.83	−1.51	−1.83		2.46	
		0.60[c,f]						
H_2ZN·**10**	0.44	0.28	−0.79	−1.39	−1.82		2.10	
ZnH_2·**10**	0.52[c]	0.21	−0.78	−1.52[c]	−1.91		2.12	
Zn_2·**10**		0.24	−0.80	−1.63[c]				
H_4·**11**		0.41[c]	−0.82	−1.51	−1.81		2.42	
		0.54[c,f]						
ZnH_2·**11**	0.51	0.23	−0.70	−1.58[c]	−2.08[c]			
H_2Zn·**11**	0.48	0.29	−0.79	−1.70[c]	−1.80[c]		2.09	
Zn_2·**11**	0.53[c]	0.35	−0.80	−1.30	−2.11[c]			*d*
H_2·**16**		0.56			−1.88	−2.26	2.44	*e*
H_2·**16**	0.75[c]	0.39			−1.82		2.21	
Zn·**16**		0.29			−2.13		2.42	*e*
Zn·**16**	0.47	0.21			−2.05		2.26	
H_2·**17**		0.33	−0.97	−1.90[c]	−2.35		2.68	*e*
H_2·**17**	0.65	0.47	−0.82	−1.49	−1.92		2.39	
Zn·**17**		0.65[c]	−0.91	−1.80[c]	−2.01	−2.26	2.66	*e*
Zn·**17**	0.48	0.30[c]	−0.80	−1.57[c]				*b*

[a] Redox potentials taken as average of anodic and cathodic peak potentials in cyclic voltammetry and are reported vs Fe/Fe^+. See text for details. [b] Contains electroactive impurity. [c] Irreversibale; E_{peak} reported. [d] Slightly soluble—evidence for adsorption. [e] Solvent = THF (0.1 M $Bu_4N^+BF_4^-$, Pt electrode). [f] Shows two waves.

free-base porphyrins (including the monomer H_2·**16** and dimers H_4·**1**, H_4·**2** discussed below) are typically 180–230 mV more positive than those for the corresponding zinc complex. For instance, the potential separation between the first oxidation and first reduction in monomers H_2·**16** and Zn·**16** (2.21 and 2.26 V, respectively) matches the empirically derived value of 2.25 ± 0.15 V for a series of octaethylporphyrin complexes undergoing ring-localized redox processes.[56] Indeed, on the whole, the potentials we observe are completely consistent with those reported by Furhop et al. for free base and zinc-complexed octaethylporphyrin in butyronitrile and in DMSO.[56]

The results obtained for monomers H_2·**16** and H_2·**17** in THF are qualitatively similar to those in CH_2Cl_2 except that the potential separation between porphyrin oxidation and reduction is greater (e.g. for compound Zn·**16**, 2.42 in THF vs 2.26 V in CH_2Cl_2). This undoubtedly reflects differences in solvation of the reduced and oxidized porphyrins in the two solvents. Kadish et al. have in fact reported a general correlation between metalloporphyrin reduction potentials and solvent properties; reduction of tetraphenylporphyrinatozinc(II) in THF occurs at the most negative potential of any solvent tested.[57] We are interested primarily in the relative redox potentials for the series **1**–**15**, and so the remaining discussion will focus on data taken in a single solvent (CH_2Cl_2).

In the monomeric systems, synthetic introduction of a quinone substituent (to give, e.g., **17**) has two primary effects: (1) The potential for porphyrin oxidation is shifted positive by 80–90 mV for both the free-base and zinc complexes; and (2) the potential separation between the first porphyrin-based oxidation and reduction increases substantially (for example to 2.39 V in compound H_2·**17** compared to 2.21 V in H_2·**16**). The electrochemical signature of the quinone group is also clearly seen in the two voltammetric waves around −0.80 V (reversible) and −1.50 (quasi-reversible) arising from reduction to the semiquinone and quinone dianion, respectively. It seems likely that the coulombic effect of the quinone dianion that would be produced upon reduction renders the corresponding porphyrin reduction more difficult (i.e., shifting the wave to a more negative redox potential). In general, these data agree with previous work[58] in supporting a model in which porphyrin and quinone redox processes occur independently, with relatively little interaction other than inductive or coulombic effects.

b. Dimers. Extension of the above results to the dimers H_4·**1**, H_4·**2**, H_4·**10**, and H_4·**11** and their mono- and bis-zinc chelates was complicated to a certain extent by the low solubility and adsorptive properties of some of these compounds in CH_2Cl_2. In addition, we also experienced some occasional difficulties in obtaining reversible voltammograms, especially for oxidation of free-base dimers and reduction of quinone-substituted zinc complexes. By and large, however, the voltammetry for many of these dimers was well behaved (as illustrated in Figure 15 for compounds H_2Zn·**10** and H_2Zn·**11**), allowing for the compilation of the data listed in Table VI. These data provide a reasonable framework with which to discuss the redox properties of the gable and flat dimers.

The gable series of 1,3-disubstituted dimers (i.e., H_4·**1** and H_4·**10**) is best described as consisting of non-interacting redox centers under the conditions of the experiment. In fact, inspection of Table VI shows that for each compound in the series, the potentials for the first porphyrin-based oxidation and reduction are within 30 mV of the values predicted from the corresponding monomers. This is not unexpected: There is minimal coupling between the 1,3-positions on the common phenyl ring, and the porphyrin subunits are sterically constrained to be noncoplanar with the phenyl bridge, as confirmed by X-ray crystallography (Figure 3). We are unable as yet to assign an electron stoichiometry to any of these waves; however, it seems likely that at least for the zinc/free base heterodimers (compounds ZnH_2·**10**, H_2Zn·**10**, and ZnH_2·**1**), each of the observed redox processes is probably a single-electron localized event.

The results for the flat series of dimers (i.e. H_4·**2** and H_4·**11**) have been somewhat more difficult to interpret. Dimer H_2Zn·**11**

(56) Furhop, J. H.; Kadish, K. M.; Davis, D. G. *J. Am. Chem. Soc.* **1973**, *95*, 5140–5147.

(57) Kadish, K. M.; Cornillan, J. L.; Yao, C. L.; Malinski, T.; Gritzner, G. *J. Electroanalytical. Chem.* **1987**, *235*, 189–207.

(58) (a) Wilford, J. H.; Archer, M. D.; Bolton, J. R.; Ho, T. F.; Schmidt, J. A.; Weedon, A. C. *J. Phys. Chem.* **1985**, *89*, 5395–5398. (b) Archer, M. D.; Gadzekpo, V. P. Y.; Bolton, J. R.; Schmidt, J. A.; Weedon, A. C. *J. Chem. Soc., Faraday Trans. 2* **1986**, *82*, 2305–2313. (c) Schmidt, J. A.; Liu, J.-Y.; Bolton, J. R.; Archer, M. D.; Gadzekpo, V. P. Y. *J. Chem. Soc., Faraday Trans. 1* **1989**, *85*, 1027–1041.

shows well-behaved cyclic voltammetry (Figure 15a), and is easily interpreted as resulting from noninteracting redox centers. The corresponding nonsubstituted heterodimer ZnH_2·**2**, on the other hand, shows a redox potential for the first oxidation that is considerably more positive than that observed for any of the corresponding monomeric zinc complexes. This generalization was also found to hold for the corresponding zinc and free-base homodimers, H_4·**2** and Zn_2·**2**, respectively; the first porphyrin reduction and oxidation waves for these compounds are both shifted positive by 70–100 mV relative to the values predicted from the monomers. This presumably reflects some degree of coupling between the porphyrin subunits. However, more definitive conclusions must await the acquisition of more precise data from systems where adsorption and solubility difficulties are minimal.

Conclusion

A number of monomeric and dimeric (both gabled and flat) porphyrins, with and without appended quinone groups have been prepared and characterized. Those dimers bearing only a single quinone substituent were also prepared as their regioselectively monometalated monozinc adducts starting from either the quinone or hydroquinone precursors as appropriate.

Complete X-ray crystallographic structural analyses were performed on three of the porphyrins reported here. These structures reveal key features of the overall molecular geometries of both the monomers and the flat and gable series of dimers. In addition, these structures indicate that, in both the monomers and dimers, the porphyrin rings are nearly perpendicular to their meso substituents.

The complex splitting pattern observed for the bridging phenyl protons in the ^1H NMR spectra of the transversely substituted, nonmetalated flat dimers provides evidence for slow subunit rotations at room temperature. Proton NMR spectroscopy also shows evidence of two different sets of pyrrole N–H signals in the monosubstituted gable and flat unmetalated dimers and was used to assign the regiochemistry of products H_2Zn·**10**, ZnH_2·**10**, H_2Zn·**11**, and ZnH_2·**11**, obtained as the result of selective metal insertions. ^{13}C NMR spectroscopy was used to characterize many of these new porphyrins and to identify the presence of a quinone functionality after DDQ oxidation.

UV–visible spectra showed the presence of excitonic interaction between the porphyrin subunits in the gable-type dimers and, to a lesser extent, in the flat series.

From electrochemical analyses it was found that: (a) The radical cation of the zinc complex of a given porphyrin is more energetically accessible (less positive redox potential) than that of the corresponding free base; (b) substitution of a porphyrin macrocycle with quinone results in a positive shift of the potential for porphyrin oxidation, while the quinone dianion gives a negative shift in the potential for porphyrin reduction; (c) model compounds containing covalently linked porphyrins and quinones are well described as consisting of nearly noninteracting subunits under electrochemical conditions. This latter generalization was found to hold very well for the quinone-substituted monomers and gable series of dimers, and less well for the flat dimers.

In summary, we believe that the combination of multiple chromophoric units and detailed electronic and structural information makes several of the new compounds reported here suitable photosynthetic models for the study of energetic and orientation effects in multistep, long-range electron transfer processes. Indeed, these flat and gable dimers are the first structurally characterized synthetic systems that may be modified so as to define an energetic arrangement ([distal porphyrin]–[proximal porphyrin]–[quinone]) possibly analogous to the Sp–Bchl–Bph sequence observed in natural bacterial photosynthetic reaction centers.

Experimental Section

General Information. Melting points were measured on a Mel-temp apparatus and are uncorrected. Electronic spectra were recorded on a Beckman DU-7 spectrophotometer. Proton and ^{13}C NMR spectra were obtained in $CDCl_3$ with either Me_4Si or $CHCl_3$ (δ = 7.24 ppm for ^1H; 77.0 ppm for ^{13}C) as an internal standard. Proton spectra were recorded on either a Varian EM-390 (90 MHz), Nicolet NT-360 (360 MHz), General Electric QE-300 (300 MHz), or Nicolet NT-500 (500 MHz) spectrometer. Unless otherwise noted, the peak assignments given were made on the basis of integrations and spectral intercomparisons with similar compounds. Carbon spectra were measured at 75, 90, or 125 MHz with use of, respectively, either a General Electric QE-300, Nicolet NT-360, or Nicolet NT-500 spectrometer. Routine low-resolution mass spectra (MS) were measured with either a Finnigan-MAT 4023 or Bell and Howell 21-491 instrument. High-resolution mass spectra (HRMS) were obtained with a Bell and Howell 21-110B instrument. Fast atom bombardment mass spectra (FAB MS) were determined with either a Kratos MS-50 instrument and a glycerol/oxalic acid matrix, or a Finnigan-MAT TSQ-70 instrument and 3-nitrobenzyl alcohol matrix. In general, the glycerol/oxalic acid matrices tended to produce molecular ion peaks 3–6 amu higher than calculated.[59] Elementary analyses were performed by Galbraith Laboratories, Knoxville, TN.

Cyclic voltammetry was performed in dichloromethane on a PAR 173/175 potentiostat with 0.2 M $[Bu_4N]/[BF_4]$ supporting electrolyte. All potentials were measured against an aqueous Ag/AgCl reference electrode but are reported vs ferrocene/ferricinium to eliminate junction potentials and to facilitate comparison with other solvent systems. Under the conditions above, $E°(Fc/Fc^+)$ = 0.58 V vs Ag/AgCl. A glassy carbon working electrode was used and was polished with either 1-μm diamond paste or 0.3-μm alumina, rinsed thoroughly, and subjected to a sequence of background scans (+1.1 to −2.3 V vs Fc/Fc^+) in order to establish a stable baseline prior to each series of measurements. All solutions were purged and blanketed with dry argon to remove dissolved oxygen.

Materials. All solvents and chemicals were of reagent grade quality, purchased commercially and used without further purification except as noted below. CH_2Cl_2 for use in the BBr_3 demethylations was heated at reflux with and distilled from P_2O_5. CH_2Cl_2 for use in electrochemical studies was heated at reflux with and distilled from CaH_2. Phosphorus oxychloride was heated at reflux with and distilled from PCl_5 directly prior to use. Dimethylformamide (DMF) was distilled under reduced pressure and stored over 4-Å molecular sieves. 1,8-Diazabicyclo-[5.4.0]undec-7-ene (DBU) was distilled under reduced pressure prior to use, unless received from Aldrich Chemical Co., in which case it was of sufficient purity to be used directly. Tetra-*n*-butylammonium fluoroborate was purified by recrystallization from ethyl acetate/pentane. Merck type 60 (230–400 mesh) silica gel was used for column chromatography. Thin-layer chromatography (TLC) was performed on commercially prepared silica gel plates purchased from Analtech, Inc.

Crystal Growth of H_2·20, Cu_2·5, and Cu_2·9. Crystals of H_2·**20** were grown at 4 °C by layering a concentrated solution of H_2·**20** in $CHCl_3$ with hexane. Crystals of Cu_2·**5** and Cu_2·**9** were obtained at room temperature by vapor diffusion of methanol into the respective chloroform solutions. For the Cu dimers these crystallization procedures introduced solvent molecules into the crystal structures. The extent and nature of these solvent molecules were deduced from the structural studies.

X-ray Structure of H_2·20. A single crystal of H_2·**20** was mounted in the cold stream ($t \approx -150$ °C at the crystal) of a CAD4 diffractometer. Preliminary data showed symmetry and systematic absences consistent with the centrosymmetric monoclinic space group C^5_{2h}–$P2_1/c$. Details of data collection are given in Table V. The structure was solved by using the program SHELXS-86.[60] All non-hydrogen atoms were located immediately and 2-fold rotational disorder about the C(20)–C(21) bond was apparent. Difference-electron density maps were used to locate the hydrogen atoms. These hydrogen atom positions were idealized (d(C–H) = 0.95 Å; B(H) = B_{eq}(C) + 1 Å^2) and were fixed in subsequent calculations. In the final cycle of refinement on F_o^2 all 5898 unique F_o^2 values were used. This cycle involved 434 variables, including anisotropic thermal parameters for the non-hydrogen atoms and an occupancy factor to describe the rotational disorder of the quinone ring. This ring has two orientations in the ratio 0.66:0.34. Only the major orientation is shown in Figure 2. This cycle converged to $R(F_o^2)$ = 0.10. Further details are in Table V. Table SIV[48] presents the final positional parameters of the non-hydrogen atoms. Table SV[48] gives the parameters for the hydrogen atoms. Table SVI[48] presents anisotropic thermal parameters. Table SVII[48] presents $10|F_o|$ vs $10|F_c|$.

X-ray Structure of Cu_2·5. A crystal of Cu_2·**5**·$(1.5CHCl_3)$·$(0.5CH_3OH)$ was mounted in the cold stream (t = −150 °C) of a CAD4 diffractometer. Preliminary data showed no symmetry or systematic absences consistent with the triclinic space groups $P1$ and $P\bar{1}$. Details of data

(59) Musselman, B. D. Proceedings of ASMS 34th Annual Conference on Mass Spectrometry and Allied Topics, Cincinnati, OH, June 8–13, 1986; pp 659–660.

(60) Sheldrick, G. M. In Crystallographic Computing 3 (Sheldrick, G. M.; Kruger, C.; Goddard, R., Eds.), pp 175–189. Oxford University Press, London-New York, 1985.

collection are given in Table V. The structure in space group $P\bar{1}$ was solved with use of the program SHELXS-86. A difference electron density map revealed the expected atoms in the molecule along with several chlorine atoms ascribed to chloroform molecules of solvation. Several difference electron density maps and cycles of refinement yielded a fairly well ordered, completely anisotropic porphyrin molecule along with one $CHCl_3$ molecule suffering from 5-fold disorder, a half-occupancy $CHCl_3$ molecule suffering from 2-fold disorder, and a half-occupancy MeOH molecule. In the final cycle of refinement on F^2 all 11574 F_o^2 values were used. This cycle involved 1015 variables and converged to values of $R(F^2) = 0.130$ and $R(F)$ ($F_o^2 > 3\sigma(F_o^2)$) = 0.085. The following material is tabulated:[48] Table SVIII, final positional parameters for the non-hydrogen atoms, Table SIX, parameters for the hydrogen atoms; Table SX, anisotropic thermal parameters, and Table SXI, $10|F_o|$ vs $10|F_c|$.

X-ray Structure of Cu_2·9. A crystal of Cu_2·9·($2CHCl_3$) was mounted in the cold stream of a CAD4 diffractometer. Preliminary data showed no symmetry or systematic absences, consistent with the triclinic space groups $P1$ and $P\bar{1}$. Details of data collection are given in Table V.

The structure was solved in space group $P\bar{1}$ with the use of the program SHELXS-86. The solution revealed the Cu_2·9 molecule (with an imposed center of symmetry) and two $CHCl_3$ molecules in the unit cell. Refinement of the structure was straightforward. In the final model the 56 non-hydrogen atoms were allowed to vibrate anisotropically while the 48 hydrogen atoms were fixed in positions idealized from their locations on difference electron density maps and were assigned fixed isotropic thermal parameters 1 Å^2 greater than the corresponding B_{eq} values of the C atoms to which they are attached. This refinement on F^2 of 505 variables and 8318 unique data converged to the agreement indices given in Table V. In the supplementary material the following are given: Table SXII, final parameters for the non-hydrogen atoms; Table SXIII, hydrogen atom parameters; Table SXIV, anisotropic thermal parameters; and Table SXV, $10|F_o|$ vs $10|F_c|$.

The GENXCH Program. The GENXCH program is a part of the software package that comes with NMR spectrometers manufactured by the General Electric Corporation. It calculates lineshapes of NMR signals from protons undergoing A–B exchange from one site (A) to another (B). With this program, which assumes that both A and B are singlets, the frequencies, linewidths, and relative amounts (%A = 100 − %B) of the two signals are entered. The mean lifetime is then varied until the calculated lineshape most closely resembles the observed lineshape. The exchange rate (k_{ex}) is then taken as the inverse of the mean lifetime τ. An Arrhenius plot (log k_{ex} vs 1/temperature (in kelvins)) then gives a line whose slope is proportional to the activation barrier E_a for the A–B exchange process. For H_4·**4** and H_4·**6**, application of the GENXCH program to the pairs of singlets in Figures 7 and 8 was complicated by the presence of the nested doubled doublets, which caused interference at around 50 °C. Nonetheless, the values obtained for this process are considered accurate to within about ±20%. Table SXVI gives the mean lifetimes in seconds for the bridging phenyl protons undergoing exchange in compounds H_4·**4** and H_4·**6**; Supplementary Figures 1 and 2 show the corresponding Arrhenius plots.

4-Nitro-3-pentanol.[61] Propionaldehyde (174 g, 3 mol), isopropyl alcohol (400 mL), and finely ground KF (25 g, 0.15 mol) were added to a three-necked round-bottomed flask equipped with a mechanical stirrer, a thermometer, a dropping funnel, and a drying tube. Nitroethane (225.2 g, 3 mol) was added dropwise with stirring, while the temperature of the solution was kept below 40 °C with the aid of an ice bath. Fairly vigorous stirring was continued for 24 h. The catalyst was then removed by filtration and the filtrate concentrated under reduced pressure. The residue was poured into water (500 mL) and the oil extracted with ether (3 × 300 mL). The ethereal layer was then dried over anhydrous Na_2SO_4, and the solvent was removed under reduced pressure. The remaining liquid was distilled in vacuo and the fraction boiling at 82–84 °C (5 Torr) was collected in a tared 1-L round-bottomed flask to afford 4-nitro-3-pentanol (320 g, 2.4 mol, 80%). The flask containing the product was used directly in the next step.

3-Acetoxy-2-nitropentane.[62] To the above flask, containing 4-nitro-3-pentanol (320 g, 2.4 mol) was added a magnetic stir egg and 1 mL of concentrated sulfuric acid. The contents of the flask were then stirred in an ice bath, and acetic anhydride (255 g, 2.5 mol) was added in portions, keeping the temperature of the reactants below 60 °C. When the addition of acetic anhydride was complete, the contents of the flask were stirred for one additional hour. The flask was then equipped for vacuum distillation. The lower boiling components (Ac_2O and AcOH) were removed with a water aspirator by gently heating (≤100 °C bath temperature) the stirred contents of the flask. After these byproducts were removed, the system was cooled, hooked up to a vacuum pump, and carefully heated. The fraction boiling at 90 °C (5 Torr) was collected, affording 3-acetoxy-2-nitropentane (370 g, 2.1 mol, 89%).

2-(Ethoxycarbonyl)-3-ethyl-4-methylpyrrole (23). To a stirred solution of 3-acetoxy-2-nitropentane (182.3 g, 1.04 mol) and ethyl isocyanoacetate (98 g, 0.87 mol) in THF (620 mL)/IPA (250 mL) was added DBU (294 g, 1.93 mol) in portions while cooling in an ice bath so as to maintain a temperature of 20–30 °C at all times. When the DBU addition was complete the orange solution was stirred for 4 h at room temperature. The solution was then filtered to remove the nitrite salt, and the solvent was removed on a rotary evaporator (50 °C bath temp, water aspirator). The residue was poured into a 1-L beaker and diluted with acetic acid (60 g, 1 mol), followed by warm water (350 mL). Additional water was then added to the point where the solution remained cloudy, even after thorough stirring. Methanol (150 mL) was then added, and the clear solution thus obtained was covered and placed in the freezer for 12 h. The resulting precipitate was collected by filtration through a Buchner funnel, washed with 60/40 (v/v) water/methanol (3 × 200 mL), and dried to give the crude product as white flakes (102.3 g, 65%), mp 73–75 °C. This crude product may be used as is, or recrystallized from methanol to give pure material, mp 76 °C (lit.[46b] mp 76 °C).

Bis(4-ethyl-3-methyl-2-pyrryl)(2,5-dimethoxyphenyl)methane (35). In a 1-L round-bottomed flask equipped with a sidearm was dissolved 2,5-dimethoxybenzaldehyde (10 g, 0.06 mol) and pyrrole **23** (21.9 g, 0.12 mol) in 80 mL absolute ethanol with stirring. The flask was purged with N_2 and *p*-toluenesulfonic acid (*p*-TsOH) (0.5 g) was added. The flask was then capped with a condenser and heated at reflux for 2 h under N_2 with magnetic stirring. At the end of this time, TLC indicated complete conversion to what was presumed to be **34**. The condenser was then removed and the ethanol solvent was evaporated from the flask by means of an N_2 stream blown through the sidearm. When the ethanol was completely evaporated, ethylene glycol (500 mL) and NaOH (15 g, 0.375 mol) were added and the oil bath replaced with a heating mantle. This mixture was held at reflux for 1 h under N_2, at a solution temperature of at least 180 °C. Next the heating mantle was removed and the flask was allowed to cool with vigorous stirring to room temperature. The solid was collected by filtration through a coarse fritted glass filter, washed with water, and dried to give pure **35** (20.8 g, 94.6%): mp 128–130 °C; ^{1}H NMR δ 1.2 (t, 6 H, CH_2CH_3), 1.8 (s, 6 H, CH_3), 2.4 (q, 4 H, CH_2CH_3), 3.6 and 3.7 (s, s, 3 H, 3 H, OCH_3), 5.7 (s, 1 H, CH), 6.3 (br s, 2 H, pyrrole CH), 6.6–6.9 (m, 3 H, phenyl ring), 7.6 (br s, 2 H, pyrrole NH); MS *m/e* 366 (48), 351 (35), 258 (100), 226 (49); HRMS calcd for $C_{23}H_{30}N_2O_2$ 366.23071, found 366.23140.

Bis(4-ethyl-5-formyl-3-methyl-2-pyrryl)(2,5-dimethoxyphenyl)methane (36). The dipyrromethane **35** (20 g, 0.055 mol) was placed in a 250-mL three-necked round-bottomed flask equipped with a N_2 inlet, dropping funnel, stir bar, and thermometer. Dry DMF (80 mL) was added and the dipyrromethane dissolved. The solution was then cooled to −20 °C in a CCl_4/dry ice slush bath. Phosphoryl chloride (26.1 g, 16 mL, 0.17 mol) was then dropped into the stirred solution under N_2 at a temperature between −20 °C and −10 °C. After the addition was complete, the solution was stirred for 1 h while its temperature was allowed to rise to ca. 25 °C. The solution was then poured into water (500 mL) and made basic with 50% NaOH. The resulting tar was collected on a glass rod and cooled until solid. The solid was triturated in hot methanol (60 mL) containing NaOH (1 g). The resulting slurry was cooled, filtered, and washed with methanol to give the crude product. Recrystallization from $CHCl_3$/MeOH gave the pure product (22.6 g, 95.5%): mp 208–210 °C; ^{1}H NMR δ 1.28 (t, 6 H, CH_2CH_3), 1.85 (s, 6 H, CH_3), 2.67 (q, 4 H, CH_2CH_3), 3.67 (s, 3 H, OCH_3), 3.70 (s, 3 H, OCH_3), 5.79 (s, 1 H, CH), 6.62 (s, 1 H, phenyl C-6), 6.82 (dd, 2 H, phenyl C-3 and C-4), 9.2 (br s, 2 H, NH), 9.55 (s, 2 H, CHO); MS *m/e* 422 (100), 393 (55), 365 (26); HRMS calcd for $C_{25}H_{30}N_2O_4$ 422.2205, found 422.2195.

Bis(4-ethyl-5-formyl-3-methyl-2-pyrryl)(2,4,6-dimethoxyphenyl)methane (45). 2,4,6-Trimethoxybenzaldehyde (1 g, 5.1 mmol) and pyrrole **23** (1.85 g, 10.2 mmol) were dissolved in methanol (8 mL) in a three-necked 100-mL round-bottomed flask equipped with a condenser, N_2 inlet, and thermometer. *p*-Toluenesulfonic acid (25 mg) was added and the flask contents held at reflux for 1 h under N_2. The methanol was then removed by a gentle stream of N_2 blown through the flask. Ethylene glycol (50 mL) and NaOH (1.5 g, 38 mmol) were then added to the flask. The gentle N_2 flow was resumed. The flask contents were held at 180 °C for 10 min and then cooled. The ethylene glycol was poured off and the crude intermediate compound **44** was dissolved in hexane (75 mL). The hexane solution was washed with water (3 × 50 mL) and dried (Na_2SO_4), and the hexane was removed on a rotary evaporator to give **44** (1.9 g, 4.8 mmol, 94%) as a highly air- and light-sensitive brown glass. Compound 44 was immediately dissolved in dry DMF (10 mL) and transferred to a 50-mL three-necked round-bottomed flask equipped with

(61) Kambe, S.; Yasuda, H. *Bull. Chem. Soc. Jpn.* **1968**, *41*, 1444–1446.
(62) Tindall, J. B. *Ind. Eng. Chem.* **1941**, *33*, 65.

a thermometer and a N_2 inlet. Nitrogen was gently blown through the flask while the contents were cooled to −10 °C with a dry ice/acetonitrile slush bath. Phosphorus oxychloride (1.3 mL, 14.4 mmol) was then added dropwise at −10 °C. The solution was stirred for an additional 30 min as it warmed to room temperature. The solution was then poured into cold water (50 mL) and made basic with 50% NaOH. The crude product was allowed to harden and was then washed with water. Recrystallization from MeOH/$CHCl_3$ gave product **45** as light brown crystals (0.8 g, 1.8 mmol, 37%): mp 203–205 °C; ^{1}H NMR δ 1.17 (t, 6 H, CH_2CH_3), 1.79 (s, 6 H, CH_3), 2.67 (q, 4 H, CH_2CH_3), 3.76 (s, 6 H, OCH_3), 3.81 (s, 3 H, OCH_3), 6.06 (s, 1 H, CH), 6.18 (s, 2 H, phenyl), 9.04 (br s, 2 H, NH), 9.48 (s, 2 H, CHO); MS *m/e* 452 (100), 422 (19), 316 (95), 285 (45). HRMS calcd for $C_{26}H_{32}N_2O_5$ 452.2311, found 452.2368.

1,4-Bis[bis[5-(ethoxycarbonyl)-4-ethyl-3-methyl-2-pyrryl]methyl]benzene (39). Terephthalaldehyde (1 g, 7.46 mmol) and pyrrole **23** (5.4 g, 29.8 mmol) were dissolved in 100 mL of absolute ethanol. Concentrated HCl (5 mL) was then added, and the solution was heated at reflux for 10 h under N_2. The resulting suspension was cooled, filtered, and washed with ethanol. Drying in vacuo gave pure **39** (5.6 g, 91%) as a white powder: mp 237 °C; ^{1}H NMR δ 1.1 (t, 12 H, CH_2CH_3), 1.25 (t, 12 H, OCH_2CH_3), 1.8 (s, 12 H, CH_3), 2.7 (q, 8 H, CH_2CH_3), 4.2 (q, 8 H, OCH_2CH_3), 5.5 (s, 2 H, CH), 7.1 (s, 4 H, phenyl ring), 8.6 (br s, 4 H, NH); MS *m/e* 822 (100); HRMS calcd for $C_{48}H_{62}N_4O_8$ 822.45677, found 822.45772.

1,3-Bis[bis[5-(ethoxycarbonyl)-4-ethyl-3-methyl-2-pyrryl]methyl]benzene (37). Isophthalaldehyde (0.335 g, 2.5 mmol) and pyrrole **23** (1.81 g, 10 mmol) were dissolved in 50 mL of absolute ethanol. Concentrated HCl (1 mL) was then added, and the solution was heated at reflux for 10 h under N_2. The resulting suspension was cooled overnight at 4 °C. It was then filtered and washed with ethanol. Drying in vacuo gave pure **37** (1.92 g, 93%) as a white powder: mp 178–180 °C; ^{1}H NMR δ 1.08 (t, 12 H, CH_2CH_3), 1.31 (t, 12 H, OCH_2CH_3), 1.74 (s, 12 H, CH_3), 2.72 (q, 8 H, CH_2CH_3), 4.25 (q, 8 H, OCH_2CH_3), 5.86 (s, 2 H, CH), 6.83 (1 H, s, Ar), 7.00 (2 H, d, Ar), 7.29 (1 H, t, Ar), 8.28 (4 H, s, NH); MS *m/e* 822 (72), 776 (100), 730 (66).

1,4-Bis[bis(4-ethyl-3-methyl-2-pyrryl)methyl]benzene (40). The tetraester **39** (5.6 g, 6.8 mmol) was held at reflux (≥180 °C) in a solution of NaOH (10 g, 0.25 mol) in ethylene glycol (500 mL) for 45 min under a N_2 flow. The solution was then cooled with vigorous stirring to room temperature. The precipitate was collected by filtration, washed with water, and dried to give the pure product as a tan powder (3.4 g, 93.4%): mp 162–3 °C. ^{1}H NMR δ 1.1 (t, 12 H, CH_2CH_3), 1.75 (s, 12 H, CH_3), 2.4 (q, 8 H, CH_2CH_3), 5.4 (s, 2 H, CH), 6.4 (br s, 4 H, pyrrole CH), 7.1 (s, 4 H, phenyl ring); 7.3 (br s, 4 H, pyrrole NH). MS *m/e* 534 (46), 425 (100). HRMS calcd for $C_{36}H_{46}N_4$ 534.37225, found 534.37343.

1,3-Bis[bis(4-ethyl-3-methyl-2-pyrryl)methyl]benzene (38). The tetraester **37** (22 g, 26.7 mmol) was added to a 5-L three-necked round-bottomed flask equipped with a paddle stirring apparatus, heating mantle, reflux condenser, and N_2 inlet. To the flask was then added ethylene glycol (2.0 L), NaOH (20 g, 500 mmol), and water (50 mL). The N_2 flow was commenced and the contents of the flask brought to reflux with stirring. Atmospheric oxygen must be excluded while the contents are heated. After 3.0 h at reflux the heating mantle was replaced by an ice bath. The product precipitated from solution and collected on the paddle as the temperature dropped. The solids obtained from the reaction were separated by filtration and were dissolved in hexane (300 mL). The hexane solution was then dried with Na_2SO_4 and filtered through Celite. The resulting clear yellow-brown solution was evaporated to dryness, first on a rotary evaporator, then under high vacuum, to give the product as a glass (12.4 g, 87%): mp 65 °C dec; ^{1}H NMR δ 1.10 (t, 12 H, CH_2CH_3), 1.70 (s, 12 H, CH_3), 2.37 (q, 8 H, CH_2CH_3), 5.36 (s, 2 H, CH), 6.29 (br s, 4 H, pyrrole CH), 6.88 (s, 2 H, phenyl ring), 6.98 (s, 1 H, phenyl ring), 7.11 (s, 1 H, phenyl ring); MS *m/e* 534 (47), 425 (84), 316 (100); HRMS calcd for $C_{36}H_{46}N_4$ 534.37225, found 534.3713.

[5-(2,8-Diethyl-3,7,12,18-tetramethyl-13,17-di-*n*-propylporphyrinyl)]benzene (H_4·16). The α-free dipyrromethane **42** (0.85 g, 2.77 mmol) and the diformyl dipyrromethane **30** (0.85 g, 270 mmol) were dissolved in a 2:1 MeOH/THF solution (200 mL) and degassed with N_2. Perchloric acid (70%, 0.5 mL) was added and the flask was stirred in the dark for 12 h. The solution was then neutralized with $NaHCO_3$ in water and the organic components were extracted into chloroform. *o*-Chloranil (0.5 g, 4 mmol) in chloroform (10 mL) was added and the solution was stirred for 1 h. A saturated solution of zinc acetate in methanol (10 mL) was then added, and the chloroform solution was heated at reflux for 20 min. After the solution was cooled, the product was washed with saturated $NaHCO_3/H_2O$, dried over Na_2SO_4, and concentrated to 10 mL on a rotary evaporator. The crude product was then redissolved in chloroform (30 mL) and passed through a 3 × 50 cm column of silica gel ($CHCl_3$). The fast running pink fraction was collected, concentrated to dryness on a rotary evaporator, and demetalated by stirring in 6:1 (v/v) trifluoroacetic acid/water (10 mL) for 12 h. The solution was then poured into chloroform (50 mL) and washed with saturated $NaHCO_3$ until neutral. The chloroform layer was dried over Na_2SO_4, concentrated to 10 mL on a rotary evaporator, and eluted through a 2 × 40 cm silica gel column ($CHCl_3$). The main band was collected and recrystallized, first from $CHCl_3$/MeOH and then from $CHCl_3$/hexane, to yield the product as a purple crystalline solid (330 mg, 20%): ^{1}H NMR δ −3.2 (br s, 2 H, NH), 1.34 (t, 6 H, $CH_2CH_2CH_3$), 1.81 (t, 6 H, CH_2CH_3), 2.39 (sextuplet, 4 H, $CH_2CH_2CH_3$), 2.51 (s, 6 H, CH_3), 3.68 (s, 6 H, CH_3), 4.06 (m, 8 H, $CH_2CH_2CH_3$ and CH_2CH_3), 7.78 (m, 3 H, phenyl H-3, H-4, H-5), 8.12 (d, 2 H, phenyl H-2, H-6), 9.97 (s, 1 H, meso), 10.20 (s, 2 H, meso); ^{13}C NMR δ 11.86, 14.55 (double), 17.59, 19.95, 26.17, 28.49, 95.67, 96.43, 127.58, 128.26, 133.17, 136.26, 139.95, 141.89, 142.87, 143.80, 144.22, 145.92; MS *m/e* 582 (100) (calcd for $C_{40}H_{46}N_4$ 582); UV–vis λ_{max} (log ε) 404 (5.38), 503 (4.31), 537 (4.01), 571 (3.99), 623 (3.66). Anal. Calcd for $C_{40}H_{46}N_4$: C, 82.43; H, 7.96; N, 9.61. Found: C, 82.73; H, 7.90; N, 9.64. For Zn·**16**: UV–vis λ_{max} (log ε) 405 (5.60), 535 (4.32), 571 (4.21).

1,4-Bis[5-(13,17-di-*n*-butyl-2,8-diethyl-3,7,12,18-tetramethylporphyrinyl)]benzene (H_4·2). The diformyl dipyrromethane **33** (4.36 g, 12.7 mmol) and the 1,4-phenyl-linked α-free dipyrromethane **40** (3.41 g, 6.4 mmol) were dissolved in hot THF (200 mL) and diluted to 1200 mL with methanol. The solution was bubbled with N_2 for 5 min, and perchloric acid (70%, 5 mL) was then added. The solution was allowed to sit in the dark for 24 h. It was then neutralized with saturated NaOAc in methanol, and a solution of *o*-chloranil (2.35 g, 9.5 mmol) in methanol (25 mL) was added. The mixture was stirred for 30 min and partitioned between water and chloroform. The chloroform layer was washed several times with 5% Na_2CO_3/H_2O (3 × 200 mL). A saturated solution of zinc acetate in methanol (40 mL) was added, the solution was heated at reflux for 20 min, and it was then washed with 5% Na_2CO_3/H_2O (100 mL) and water (3 × 200 mL). The solution was then dried over Na_2SO_4 and concentrated to ca. 50 mL on a rotary evaporator. After sitting for several hours, the solution was filtered through a medium frit and the pink solid (ca. 160 mg) which separated was dissolved in concentrated sulfuric acid (30 mL) in a 1-L separatory funnel. Chloroform (300 mL) was added, followed by water (300 mL) (*Caution! Exothermic!*). The funnel was stoppered and slowly inverted so as to prevent immediate recombination of the sulfuric acid and water layers. After venting once, the funnel was then shaken and vented several times. The chloroform layer was removed and the aqueous layer was extracted with 100 mL portions of chloroform until colorless. The chloroform layers were combined and neutralized by stirring with 5% Na_2CO_3 solution for 20 min. The chloroform solution was then dried over Na_2SO_4, concentrated to 40 mL on a rotary evaporator, and passed through a 3 × 50 cm silica gel column ($CHCl_3$ eluent). The product was collected and recrystallized from $CHCl_3$/MeOH, followed by $CHCl_3$/hexanes to give the product as purple crystals, 60 mg (8%): ^{1}H NMR δ −2.9 (br s, 4 H, NH), 1.17 (t, 12 H, $CH_2CH_2CH_2CH_3$), 1.83 (sextuplet, 8 H, $CH_2CH_2CH_2CH_3$), 1.91 (t, 12 H, CH_2CH_3), 2.32 (p, 8 H, $CH_2CH_2CH_2CH_3$), 3.16 (s, 12 H, CH_3), 3.69 (s, 12 H, CH_3), 4.06 (t, 8 H, $CH_2CH_2CH_2CH_3$), 4.175 (q, 8 H, CH_2CH_3), 8.54 (s, 4 H, phenyl), 9.94 (s, 2 H, meso), 10.26 (s, 4 H, meso); ^{13}C NMR δ 11.83, 14.25, 17.67, 20.10, 23.14, 26.25, 35.27, 95.79, 96.70, 118.94, 133.81, 135.60, 136.23, 140.29, 141.68, 142.47, 143.75, 144.19, 145.11, 146.14; UV–vis λ_{max} (log ε) 413 (5.51), 506 (4.46), 540 (4.95), 574 (4.00), 625 (3.15). Anal. Calcd for $C_{78}H_{94}N_8$: C, 81.92; H, 8.28; N, 9.80. Found: C, 81.84; H, 8.35; N, 9.61. For Zn_2·2: UV–vis λ_{max} (log ε) 410 sh (5.52), 419 (5.61), 540 (4.54), 574 (4.41).

1,3-Bis[5-(13,17-di-*n*-propyl-2,8-diethyl-3,7,12,18-tetramethylporphyrinyl)]benzene (H_4·1). Compound H_4·1 was prepared in 12% yield from α-free bisdipyrromethane **38** and diformyl dipyrromethane **30** in an analogous fashion to that used to prepare flat porphyrin H_4·2: ^{1}H NMR δ −3.0 (br s, 4 H, NH), 1.22 (t, 12 H, $CH_2CH_2CH_3$), 1.72 (t, 12 H, CH_2CH_3), 2.25 (m, 8 H, $CH_2CH_2CH_3$), 3.07 (s, 12 H, CH_3), 3.55 (s, 12 H, CH_3), 3.99 (m, 16 H, $CH_2CH_2CH_3$), 7.82 (s, 1 H, phenyl H-2), 8.27 (t, 1 H, phenyl H-5), 8.90 (2 H, d, phenyl H-4 and H-6), 9.78 (s, 2 H, meso), 10.04 (s, 4 H, meso); ^{13}C NMR δ 11.8, 14.5, 17.2, 20.2, 26.1, 28.3, 34.1, 96.0, 96.4, 118.0, 125.6, 127.6, 133.8, 135.3, 136.2, 140.0, 141.0, 141.9, 143.7, 144.8, 145.2, 146.1; UV–vis λ_{max} (log ε) 407.5 (5.62), 506 (4.36), 540.5 (4.44), 575 (4.35), 627 (3.50). Anal. Calcd for $C_{74}H_{86}N_8$: C, 81.68; H, 7.97; N, 10.30. Found: C, 81.68; H, 8.11; N, 10.08. For Zn_2·1: UV–vis λ_{max} (log ε) 404.5 (5.58), 420 (5.48), 540 (4.43), 574 (4.34).

[5-[2,8,12,18-Tetraethyl-15-(2,5-dimethoxyphenyl)-3,7,13,17-tetramethylporphyrinyl]]benzene (H_2·18). The α-free dipyrromethane **42** (0.56 g, 1.83 mmol) and diformyl dipyrromethane **36** (0.77 g, 1.83 mmol) were dissolved in hot THF (30 mL) and diluted to 350 mL with methanol in a 500-mL round-bottomed flask. The flask was bubbled with N_2 for 5 min, and perchloric acid (70%, 3 mL) was added. The flask was shaken

vigorously and placed in the dark for 24 h. The contents of the flask were then neutralized with a saturated solution of NaOAc in methanol (50 mL). *o*-Chloranil (1.35 g, 5.5 mmol) in methanol (10 mL) was then added, and the contents of the flask were stirred magnetically for 1 h and then poured into a 2-L separatory funnel. Water (500 mL) and chloroform (500 mL) were added to the funnel, which was shaken and vented. The organic layer was washed several more times with water and transferred to a 1-L round-bottomed flask. Cupric acetate (1 g) was added to the flask, and the contents of the flask were heated at reflux under N_2 for 1 h. The solution was then filtered through Celite, washed with water (3 × 200 mL), dried over $MgSO_4$, concentrated to 30 mL on a rotary evaporator and then filtered through silica gel ($CHCl_3$). The red fractions containing Cu·**18** were collected and transferred to a separatory funnel. Demetalation was accomplished as follows: Sulfuric acid (3 mL) was added to the funnel, which was stoppered and shaken vigorously for 5 min. The funnel was allowed to sit for a minute so the acid would settle to the bottom, and water (100 mL) was added carefully to the funnel (*Caution! Exothermic!*). The funnel was next carefully inverted and vented and shaken and vented several more times. The chloroform was drained off, and the aqueous layer was extracted with 50-mL aliquots of chloroform until the extracts were pale. The chloroform extracts were combined and neutralized with 5% Na_2CO_3, dried over Na_2SO_4, concentrated on a rotary evaporator, and passed through a silica gel column (1% MeOH/$CHCl_3$). The product was collected and recrystallized first from $CHCl_3$/MeOH and then $CHCl_3$/hexane to give H_2·**18** (0.5 g, 40%) as a dark powder: ^{1}H NMR δ −2.35 (br s, 2 H, NH), 1.79 (t, 6 H, CH_2CH_3), 1.81 (t, 6 H, CH_2CH_3), 2.51 (s, 6 H, CH_3), 2.64 (s, 6 H, CH_3), 3.69 (s, 3 H, OCH_3), 3.88 (s, 3 H, OCH_3), 4.05 (m, 8 H, CH_2CH_3), 7.30 (m, 3 H, $C_6H_3(OCH_3)_2$), 7.76 (m, 3 H, H-3, H-4, and H-5 of C_6H_5-(porph), 8.10 (dd, 2 H, H-2 and H-6 of C_6H_5-(porph)), 10.23 (s, 2 H, meso); ^{13}C NMR δ 13.63, 14.31, 17.60, 19.96, 26.91, 56.08, 96.35, 111.90, 113.40, 115.12, 118.02, 120.37, 127.58, 128.21, 132.97, 135.63, 135.77, 140.96, 141.06, 144.45, 145.37, 153.76, 153.95; MS *m/e* 690 (100) (calcd for $C_{46}H_{50}N_4O_2$ 690); UV–vis λ_{max} (log ϵ) 409 (5.37), 507 (4.40), 541 (4.09), 574 (4.14), 626 (3.87). Anal. Calcd for $C_{46}H_{50}N_4O_2$: C, 79.96; H, 7.29; N, 8.11. Found: C, 80.03; H, 7.46; N, 7.85. For Zn·**18**: UV–vis λ_{max} (log ϵ) 411 (5.61), 540 (4.42), 576 (4.22).

[5-[2,8,12,18-Tetraethyl-15-(2,5-dihydroxyphenyl)-3,7,13,17-tetramethylporphyrinyl]]benzene (H_2·19) and [5-[15-[2′-(1′,4′-benzoquinonyl)]-2,8,12,18-tetraethyl-3,7,13,17-tetramethylporphyrinyl]]benzene (H_2·17). The bis-hydroquinone ether H_2·**18** (40 mg, 0.058 mmol) was dissolved in dry dichloromethane (5 mL) and placed in a 50-mL round-bottomed flask equipped with a N_2 inlet. BBr_3 (0.5 mL) was added and the flask was stirred in the dark under N_2 at room temperature for 3 h. The contents of the flask were diluted to 25 mL with dichloromethane. The BBr_3 was then quenched by cautious dropwise addition of methanol (*Caution! Violently exothermic!*). To the flask was then added 10% Na_2CO_3 (20 mL). The flask was stirred for 30 min, and the liquids were separated, along with a solid at the liquid/liquid interface. The organic layer and the solid were passed through a medium fritted glass filter. The organic layer was taken to dryness on a rotary evaporator. The solid, which collected on the frit, was redissolved in 5% methanol/$CHCl_3$ (20 mL) and added to the dried organic layer. The resulting solution was dried over Na_2SO_4, concentrated to 5 mL, and passed through a 1 cm × 25 cm silica gel column, with at first 5% MeOH in $CHCl_3$, and then, after the first two minor bands had eluted, 10% MeOH in $CHCl_3$ as the eluents. The slow major band was collected and concentrated to dryness on a rotary evaporator to yield the intermediate hydroquinone H_2·**19** in crude form (24 mg, 51%). This crude material was not purified further but was converted directly to the quinone H_2·**17** in quantitative yield by the following method: The hydroquinone H_2·**19** (24 mg, 0.030 mmol) was dissolved in 1% MeOH/$CHCl_3$ (2 mL) and was stirred for 5 min with a solution of DDQ (10 mg, 0.045 mmol) in 1% MeOH/$CHCl_3$ (1 mL) that contained triethylamine (1 drop). The resulting solution was passed through silica gel (1% MeOH/$CHCl_3$ eluent) and the major band was collected and recrystallized from $CHCl_3$/hexane. The product was recovered quantitatively as a purple crystalline powder: ^{1}H NMR δ −2.39 (br, 2 H, NH), 1.78 (t, 6 H, CH_2CH_3), 1.82 (t, 6 H, CH_2CH_3), 2.49 (s, 6 H, CH_3), 3.16 (s, 6 H, CH_3), 4.04 (m, 8 H, CH_2CH_3 and CH_2CH_3), 7.37 (m, 3 H, quinone C-H3, -H5, and -H6), 7.78 (m, 3 H, phenyl C-H3, -H4, and -H5), 8.06 (dd (7 Hz), 2 H, phenyl C-H2, and -H6), 10.25 (s, 2 H, meso); ^{13}C NMR δ 14.31, 16.42, 17.54, 17.63, 19.92, 19.98, 97.15, 106.22, 119.4, 127.73, 128.41, 132.79, 133.16, 136.43, 137.11, 137.86, 139.54, 141.14, 141.50, 142.00, 144.49, 144.81, 145.26, 145.59, 150.15, 187.32, 188.98; MS *m/e* calcd for $C_{44}H_{46}N_4O_2$ 662, found 666 (37), 664 (26), 662 (35), 318 (27); UV–vis λ_{max} (log ϵ) 406 (5.39), 504 (4.39), 538 (4.05), 573 (3.99), 624 (3.67). Anal. Calcd for $C_{44}H_{46}N_4O_2$·H_2O: C, 77.62; H, 7.11; N, 8.30. Found: C, 77.65; H, 6.39; N, 8.15. For Zn·**17**: UV–vis λ_{max} (log ϵ) 415 (5.62), 541 (4.40), 575 (4.17).

[5-(2,8-Diethyl-3,7,12,18-tetramethyl-13,17-di-*n*-propylporphyrinyl)]-2,5-dimethoxybenzene (H_2·21). The α-free dipyrromethane **29** (0.67 g, 258 mmol) and diformyl dipyrromethane **36** (1.09 g, 258 mmol) were dissolved in hot THF (50 mL) in a 500-mL round-bottomed flask and the solution was diluted to 450 mL with methanol. The solution was bubbled for 5 min with N_2, and then perchloric acid (5 mL) was added to the flask, which was stoppered, shaken, and placed in the dark for 24 h. The contents of the flask were then neutralized with a saturated solution of NaOAc/MeOH. *o*-Chloranil (0.95 g, 307 mmol) was then added, and the contents of the flask were magnetically stirred in the dark for 36 h. The purple suspension that resulted was separated by filtration through a medium fritted glass filter, washed with methanol, and dried to give nearly pure product (1.3 g, 78%). Samples for analysis were purified by chromatography (silica gel/$CHCl_3$ eluent) and recrystallized from $CHCl_3$/hexane: ^{1}H NMR δ −3.26 (s, 1 H, NH), −3.15 (s, 1 H, NH), 1.32 (t, 6 H, $CH_2CH_2CH_3$), 1.79 (t, 6 H, CH_2CH_3), 2.36 (sextuplet, 4 H, $CH_2CH_2CH_3$), 2.62 (s, 6 H, CH_3), 3.66 (s, 6 H, CH_3), 3.67 (s, 3 H, OCH_3), 3.87 (s, 3 H, OCH_3), 4.05 (m, 8 H, $CH_2CH_2CH_3$ and CH_2CH_3), 7.3 (m, 3 H, $C_6H_3(OCH_3)_2$), 9.94 (s, 1 H, meso), 10.16 (s, 2 H, meso); ^{13}C NMR δ 11.84, 13.81, 14.54, 17.62, 19.96, 26.16, 28.50, 56.07, 95.72, 96.28, 111.91, 114.52, 115.06, 120.57, 132.42, 135.94, 136.11, 139.81, 141.85, 143.68, 144.05, 144.41, 145.64, 153.82, 153.98; MS *m/e* calcd for $C_{42}H_{50}N_4O_2$ 642, found 642 (100); HRMS calcd 642.39338, found 642.39362; UV–vis λ_{max} (log ϵ) 404 (5.28), 503 (4.24), 538 (3.96), 571 (3.95), 623 (3.69). Anal. Calcd for $C_{42}H_{50}N_4O_2$: C, 78.47; H, 7.84; N, 8.72. Found: C, 77.91; H, 7.45; N, 8.90.

[5-(2,8-Diethyl-3,7,12,18-tetramethyl-13,17-di-*n*-propylporphyrinyl)]-2,5-dihydroxybenzene (H_2·22) and 2-[5-(2,8-Diethyl-3,7,12,18-tetramethyl-13,17-di-*n*-propylporphyrinyl)]-1,4-dioxo-2,5-cyclohexadiene (H_2·20). The hydroquinone ether H_2·**21** was demethylated and oxidized according to the procedure used to prepare quinone H_2·**17**. The yield of H_2·**20** was 70%: ^{1}H NMR δ −3.42 (s, 1 H, NH), −3.33 (s, 1 H, NH), 1.20 (t, 6 H, $CH_2CH_2CH_3$), 1.71 (t, 6 H, CH_2CH_3), 2.24 (sextuplet, 4 H, $CH_2CH_2CH_3$), 3.07 (s, 6 H, CH_3), 3.54 (s, 6 H, CH_3), 3.94 (m, 8 H, $CH_2CH_2CH_3$ and CH_2CH_3), 7.16 (s, 1 H, quinone H-6), 7.27 (dd, 2 H, quinone H-3 and H-4), 9.88 (s, 1 H, meso), 10.07 (s, 2 H, meso); UV–vis λ_{max} (log ϵ) 402.5 (5.32), 501 (4.27), 534 (4.10), 571 (3.94), 623 (3.77). Anal. Calcd for $C_{40}H_{44}N_4O_2$·H_2O: C, 78.40; H, 7.24; N, 9.14. Found: C, 78.62; H, 7.44; N, 9.12. For Zn·**20**: UV–vis λ_{max} (log ϵ) 410.5 (5.60), 538 (4.31), 575 (4.25). The X-ray crystal structure of H_2·**20** described above provides additional evidence for the structure of this compound.

1,3-Bis[5-[2,8,12,18-tetraethyl-15-(2,5-dimethoxyphenyl)-3,7,13,17-tetramethylporphyrinyl]]benzene (H_4·5). Dialdehyde **36** (0.63 g, 1.5 mmol) and α-free dipyrromethane **38** (0.4 g, 0.75 mmol) were dissolved in methanol (200 mL) in a 250-mL round-bottomed flask, and the solution was purged with N_2. Perchloric acid (70%, 2 mL) was added to the flask, which was shaken vigorously and allowed to sit in the dark for 24 h. A saturated solution of sodium acetate in methanol (20 mL) was then added followed by a solution of *o*-chloranil in MeOH (87 mg, 2.25 mmol). After it was stirred in the dark for several hours, the reaction mixture was poured into water (300 mL) and extracted with 100-mL portions of chloroform until the extracts were pale in color. After the organic layer was dried over $MgSO_4$ and filtered, a saturated solution of cupric acetate in MeOH (10 mL) was added and the mixture was heated at reflux for 20 min. The solution was cooled, washed with water (3 × 100 mL), and dried over $MgSO_4$. The solution volume was concentrated to 30 mL on a rotary evaporator and was passed through silica gel ($CHCl_3$ eluent). The fast-running red component Cu_2·**5** was collected and transferred to a separatory funnel. Concentrated H_2SO_4 (5 mL) was added, and then the funnel was stoppered and shaken vigorously for 5 min. Water (100 mL) was carefully added to the funnel, which was then restoppered, inverted, vented, and shaken and vented several more times (*Caution! Pressure buildup!*). The chloroform was drawn off and the aqueous portion was extracted with 40-mL portions of chloroform until the eluents were pale in color. The chloroform extracts were combined and neutralized with aqueous Na_2CO_3. The chloroform layer was then dried over $MgSO_4$, filtered through Celite, concentrated to 20 mL on a rotary evaporator, and eluted through silica ($CHCl_3$, eluent). The main band was collected and recrystallized from $CHCl_3$/MeOH to give pure H_4·**5** (80 mg, 8%) as a purple crystalline solid: ^{1}H NMR δ −2.12 (4 H, br s, NH), 1.73 (m, 24 H, CH_2CH_3), 2.55 (s, 12 H, CH_3), 3.08 (s, 12 H, CH_3), 3.5 to 3.9 (br m, 12 H, $C_6H_3(OCH_3)_2$), 3.98 (m, 16 H, CH_2CH_3), 7.16 (d, 4 H, H-3 and H-4 of $C_6H_3(OCH_3)_2$), 7.28 (s, 2 H, H-6 of $C_6H_3(OCH_3)_2$), 8.05 (s, 1 H, bridging phenyl H-2), 8.28 (t, 1 H, bridging phenyl H-5), 8.88 (s, 2 H, bridging phenyl H-4 and H-6), 10.11 (s, 4 H, meso); ^{13}C NMR δ 13.5, 17.2, 17.4, 17.6, 19.9, 20.0, 56.0, 96.5, 111.9, 113.6, 115.1, 117.2, 120.2, 125.5, 131.7, 133.5, 134.8, 135.6, 140.6, 140.7, 140.9, 141.9, 144.4, 144.7, 145.4, 145.8, 153.6, 153.9; FAB MS (glycerol/oxalic acid) shows a cluster of peaks at 1303–1308 amu (calcd

for $C_{86}H_{94}N_8O{\cdot}H^+$ 1304); UV–vis λ_{max} (log ϵ) 415.5 (5.53), 511.5 (4.52), 545 (4.08), 578 (4.12), 629.5 (3.15). Anal. Calcd for $C_{86}H_{94}N_8O_4$: C, 79.23; H, 7.27; N, 8.60. Found: C, 78.96; H, 7.61; N, 8.87. The X-ray structure of $Cu_2{\cdot}$**5**$\cdot(1.5CHCl_3)\cdot(0.5CH_3OH)$ (see above) provides inter alia a further characterization of $H_4{\cdot}$**5**.

1,4-Bis[5-[2,8,12,18-tetraethyl-15-(2,5-dimethoxyphenyl)-3,7,13,17-tetramethylporphyrinyl]]benzene ($H_4{\cdot}$6). The flat bis-hydroquinone ether $H_4{\cdot}$**6** was prepared from **40** and **36** in the same fashion used to prepare the gable bis-hydroquinone ether $H_4{\cdot}$**5** from **38** and **36** (yield, 8%): ^{1}H NMR δ −1.99 (s, 2 H, NH), −1.88 (s, 2 H, NH), 1.86 (t, 12 H, CH_2CH_3), 1.91 (t, 12 H, CH_2CH_3), 2.68 (s, 12 H, CH_3), 3.23 (s, 12 H, CH_3), 3.72 (s, 6 H, $C_6H_3(OCH_3)_2$), 3.90 (s, 6 H, $C_6H_3(OCH_3)_2$), 4.09 (m, 8 H, CH_2CH_3), 4.19 (q, 8 H, CH_2CH_3), 7.29 (s, 2 H, H-6 of $C_6H_3(OCH_3)_2$), 7.37 (d, 2 H, H-4 of $C_6H_3(OCH_3)_2$), 7.39 (s, 2 H, H-3 of $C_6H_3(OCH_3)_2$), 8.60 (dd (9 Hz), (porph)$_2$-C_6H_4), 10.33 (s, 4 H, meso); ^{13}C NMR δ 13.43, 17.18, 17.48, 19.83, 19.96, 55.89, 96.41, 111.74, 113.49, 114.95, 117.76, 120.13, 128.63, 130.69, 131.53, 133.27, 135.22, 135.52, 140.60, 140.87, 142.08, 144.32, 145.38, 145.55, 153.54, 153.79; FAB MS (glycerol/oxalic acid matrix) shows a cluster of peaks at 1303–1305 amu (calcd for $C_{86}H_{94}N_8O_4{\cdot}H^+$ 1303); UV–vis λ_{max} (log ϵ) 418.7 (5.72), 510 (4.66), 543 (4.32), 576 (4.35), 627 (3.90). Anal. Calcd for $C_{86}H_{94}N_8O_4$: C, 79.23; H, 7.27; N, 8.60. Found: C, 78.96; H, 7.61; N, 8.87.

1,4-Bis[5-[2,8,12,18-tetraethyl-15-(2,4,6-trimethoxyphenyl)-3,7,13,17-tetramethylporphyrinyl]]benzene ($H_4{\cdot}$9). The flat bis ether $H_4{\cdot}$**9** was prepared from **40** and **45** in the same fashion used to prepare the gable bis-hydroquinone ether $H_4{\cdot}$**5** from **38** and **36** (yield, 3%): ^{1}H NMR δ −1.95 (s, 2 H, NH), −1.84 (s, 2 H, NH), 1.85 (t, 12 H, CH_2CH_3), 1.90 (t, 12 H, CH_2CH_3), 2.72 (s, 12 H, CH_3), 3.21 (s, 12 H, CH_3), 3.58 (s, 12 H, $C_6H_2(OCH_3)_3$), 4.08 (q, 8 H, CH_2CH_3), 4.14 (s, 6 H, $C_6H_2(OCH_3)_3$), 4.17 (q, 8 H, CH_2CH_3), 6.62 (s, 2 H, $C_6H_2(OCH_3)_2$), 8.58 (s, (porph)$_2$-C_6H_4), 10.27 (s, 4 H, meso); FAB MS (3-nitrobenzyl alcohol) shows a sharp cluster of peaks at 1363–1365 amu (calcd for $C_{88}H_{98}N_8O_6{\cdot}H^+$ 1363); HRMS calcd for $C_{88}H_{98}N_8O_6{\cdot}H^+$ 1363); HRMS calcd for $C_{88}H_{98}N_8O_6{\cdot}H^+$ 1363.7688, found 1363.7427; UV–vis λ_{max} 415, 445 (sh), 508, 540, 575, 627. As with $H_4{\cdot}$**5**, the X-ray structure of $Cu_2{\cdot}$**9**$\cdot(2CHCl_3)$ (see above) provides a further proof of structure for $H_4{\cdot}$**9**.

1,3-Bis[5-[2,8,12,18-tetraethyl-15-(2,5-dihydroxyphenyl)-3,7,13,17-tetramethylporphyrinyl]]benzene ($H_4{\cdot}$7) and 1,3-Bis[5-[15-[2′-(1′,4′-benzoquinonyl)]-2,8,12,18-tetraethyl-3,7,13,17-tetramethylporphyrinyl]]-benzene ($H_4{\cdot}$3). The bis-hydroquinone ether $H_4{\cdot}$**5** (50 mg, 0.038 mmol) was dissolved in dry dichloromethane (5 mL) in a 50-mL round-bottomed flask equipped with a N_2 inlet. BBr_3 (0.5 mL) was added, and the flask was stirred in the dark under N_2 at room temperature for 3 h. The contents of the flask were then diluted to 25 mL with dichloromethane. The BBr_3 was then quenched by cautious dropwise addition of methanol (*Caution! Violently exothermic!*). To the flask was then added a 10% w/v solution of aqueous Na_2CO_3 (20 mL). The flask was stirred for 30 min, and the liquids were separated, along with a solid at the liquid/liquid interface. The organic layer and the solid were passed through a medium fritted glass filter. The organic layer was taken to dryness on a rotary evaporator. The solid, which collected on the frit, was redissolved in 5% methanol/$CHCl_3$ (20 mL) and was added to the dried organic layer. The resulting solution was dried over Na_2SO_4, concentrated to 5 mL, and passed through a 1 cm × 25 cm silica gel column, with at first 5% MeOH in $CHCl_3$, and then, after the first two minor bands had eluted, 10% MeOH in $CHCl_3$ as the eluents. The slow major band was collected and concentrated to dryness on a rotary evaporator to yield the intermediate hydroquinone $H_4{\cdot}$**7** in crude form (24 mg, 51%). This crude material was not purified further but was converted directly to the bis-quinone $H_4{\cdot}$**3** in near quantitative yield by the method described under the synthesis of $H_2{\cdot}$**17**. For $H_4{\cdot}$**7**: FAB MS (glycerol/oxalic acid matrix) shows a cluster of peaks at 1247–1251 amu (calcd for $C_{82}H_{86}N_8O_4{\cdot}H^+$ 1247). For $H_4{\cdot}$**3**: ^{1}H NMR δ −2.27 (s, 2 H, NH), −2.20 (s, 2 H, NH), 1.77 (m, 24 H, CH_2CH_3), 3.08 (s, 12 H, CH_3), 3.13 (s, 12 H, CH_3), 4.02 (m, 16 H, CH_2CH_3), 7.30 (m, 6 H, quinone), 8.05 (br s, 1 H, H-2 of (porph)$_2$-C_6H_4), 8.32 (t, 1 H, H-5 of (porph)$_2$-C_6H_4), 8.90 (br s, 2 H, H-4 and H-6 of (porph)$_2$-C_6H_4), 10.15 (s, 4 H, meso); ^{13}C NMR δ 16.2, 17.1, 17.3, 17.6, 20.0 (double), 97.2, 106.2, 118.4, 125.6, 133.0, 133.5, 135.3, 137.0, 137.8, 139.2, 140.3, 141.1, 141.3, 141.7, 144.4, 145.0, 145.5, 145.9, 149.9, 187.0, 188.8; FAB MS (glycerol/oxalic acid matrix) shows a cluster of peaks from 1243.6 to 1249.6 amu (calcd for $C_{82}H_{82}N_8O_4$ 1243.6); UV–vis λ_{max} (log ϵ) 417 (5.46), 510 (4.41), 543 (4.10), 579 (4.02), 630 (3.58). Anal. Calcd for $C_{82}H_{82}N_8O_4{\cdot}2H_2O$: C, 76.97; H, 6.77; N, 8.76. Found: C, 76.25; H, 6.58; N, 8.42. For $Zn_2{\cdot}$**3**: UV–vis λ_{max} (log ϵ) 410 (5.53), 427 (5.49), 545 (4.41), 579 (4.12).

1,4-Bis[5-[2,8,12,18-tetraethyl-15-(2,5-dihydroxyphenyl)-3,7,13,17-tetramethylporphyrinyl]]benzene ($H_4{\cdot}$8) and 1,4-Bis[5-[15-[2′-(1′,4′-benzoquinonyl)]-2,8,12,18-tetraethyl-3,7,13,17-tetramethylporphyrinyl]]-benzene ($H_4{\cdot}$4). The tetramethoxy-protected bis-hydroquinone $H_4{\cdot}$**6** (50 mg, 0.038 mmol) was demethylated with BBr_3 by the same procedure described above for the preparation of $H_4{\cdot}$**7**. In this case, the intermediate hydroquinone $H_4{\cdot}$**8** proved insoluble in most organic solvents. This complicated isolation and precluded purification. As a result, the suspension of $H_4{\cdot}$**8** in chloroform, which was obtained following quenching of the BBr_3 reaction, was treated directly with a 1.5 M excess of DDQ in the presence of Na_2SO_4. The quinone $H_4{\cdot}$**4** dissolved as it formed. When all the porphyrinic material had dissolved, the solution was filtered and concentrated to 15 mL on a rotary evaporator and was then passed through a silica gel column ($CHCl_3$ eluent). The product was recrystallized from $CHCl_3$/MeOH followed by $CHCl_3$/hexane to give product $H_4{\cdot}$**4** (35 mg, 72%) as light brown fluffy needles: ^{1}H NMR δ −1.9 (br, 4 H, NH), 1.88 (m, 24 H, CH_2CH_3), 3.19 (s, s, 24 H, CH_3), 4.14 (m, 16 H, CH_2CH_3), 7.4 (m, 6 H, quinone), 8.59 (dd, 4 H, (porph)$_2$-C_6H_4), 10.34 (s, 4 H, meso); ^{13}C NMR δ 16.33, 17.33, 17.65, 20.03, 20.10, 97.40, 106.48, 119.14, 133.33, 133.46, 133.50, 135.93, 137.18, 137.90, 139.55, 141.20, 141.34, 142.13, 144.72, 144.91, 145.71, 146.05, 150.03, 187.30, 188.93; FAB MS (3-nitrobenzyl alcohol matrix) shows a cluster of peaks at 1243–1251 amu (calcd for $C_{82}H_{82}N_8O_4{\cdot}H^+$ 1243); UV–vis λ_{max} (log ϵ) 416 (5.77), 507.5 (4.74), 540 (4.40), 576 (4.39), 625 (4.13). Anal. Calcd for $C_{82}H_{82}N_8O_4{\cdot}2H_2O$: C, 76.96; H, 6.77; N, 8.76. Found: C, 76.59; H, 6.52; N, 8.44. For $Zn_2{\cdot}$**4**: UV–vis λ_{max} (log ϵ) 421.5 (5.81), 541 (4.56), 577 (4.37).

1-[5-[2,8,12,18-Tetraethyl-15-(2,5-dimethoxyphenyl)-3,7,13,17-tetramethylporphyrinyl]]-3-[5-(2,8-diethyl-3,7,12,18-tetramethyl-13,17-di-*n*-propylporphyrinyl)]benzene ($H_4{\cdot}$12). Dialdehyde **36** (1.58 g, 3.74 mmol) and bis(5-formyl-4-methyl-3-propyl-2-pyrryl)methane[43] (**30**) (1.17 g, 3.74 mmol) were dissolved in hot THF (250 mL) in a 1-L round-bottomed flask and diluted to 700 mL with methanol. 1,3-Bis[bis(4-ethyl-3-methyl-2-pyrryl)methyl]benzene[43] (**38**) (2.00 g, 3.74 mmol) was then added and the solution was bubbled with N_2 for 5 min. Perchloric acid (3 mL) was then pipetted in, and the flask was stoppered and shaken vigorously for 1 min and then placed in the dark for 24–48 h. The acid was then neutralized with sodium acetate, and the solvent was removed on a rotary evaporator. The solid residue was taken up in chloroform (200 mL) and treated with *o*-chloranil (2.76 g, 0.011 mol). After the solution was stirred for 20 min, solid cupric acetate (1 g) was added, and the mixture was heated at reflux under N_2 for 1 h. The solution was next filtered through Celite, washed with water (3 × 200 mL), dried over $MgSO_4$, concentrated to 30 mL on a rotary evaporator, and then purified by chromatography on silica gel with $CCl_4/CHCl_3$ (1/1 v/v) as the eluent. Three red bands appeared along with trace amounts of monomeric porphyrin byproducts. These bands are in order of elution: $Cu_2{\cdot}$**1**, $Cu_2{\cdot}$**12**, and $Cu_2{\cdot}$**5**. The second red band was collected, concentrated to 200 mL, and placed in a 500-mL separatory funnel. H_2SO_4 (5 mL) was added to the funnel which was then stoppered and shaken vigorously for 5 min. The funnel was then allowed to sit for another 2–3 min. Water (100 mL) was next carefully added (*Caution! Exothermic!*). The funnel was then restoppered and slowly inverted to prevent immediate combination of the water and sulfuric acid layers. After it was vented once, the funnel was shaken and vented several times. The chloroform layer was removed, and the aqueous layer was washed several times with chloroform until colorless. The chloroform layers were combined and made basic with 5% aqueous K_2CO_3 in a stirred 500-mL Erlenmeyer flask. After the neutralization was complete, the chloroform layer was again separated, dried over Na_2SO_4, and concentrated to dryness on a rotary evaporator. The solid so obtained was dissolved in a minimum of chloroform and passed through a 3 × 50 cm silica column (1% MeOH/$CHCl_3$ eluent). The major band was collected and recrystallized from chloroform/hexane to give the product, $H_4{\cdot}$**12**, as a lustrous purple powder, 0.136 g (3%): ^{1}H NMR δ −2.95, −3.04 (s, s, 2 H, NH), −2.13 (br s, 2 H, NH), 1.24 (t, 6 H, $CH_2CH_2CH_3$), 1.73 (br m, 18 H, CH_2CH_3), 2.27 (sextuplet, 4 H, $CH_2CH_2CH_3$), 2.55 (s, 6 H, CH_3), 3.10 (s, 6 H, CH_3), 3.11 (s, 6 H, CH_3), 3.57 (s, 6 H, CH_3), 3.8–4.1 (m, 16 H, CH_2CH_3 and $CH_2CH_2CH_3$), 7.15–7.3 (m, 3 H, $C_6H_3(OCH_3)_2$), 7.96 (s, H, (porph)$_2$-phenyl), 8.29 (t, 1 H, (porph)$_2$-phenyl), 8.8–9.0 (m, 2 H, (porph)$_2$-phenyl), 9.81 (s, 1 H, meso), 10.07 (s, 2 H, meso), 10.10 (s, 2 H, meso); ^{13}C NMR δ 11.75, 13.53, 14.47, 17.18, 17.43, 17.54, 19.89, 19.99, 26.08, 28.38, 56.03, 95.87, 96.51, 96.65, 111.88, 113.61, 115.07, 117.07, 118.02, 120.20, 125.35, 131.67, 133.45, 133.54, 134.77, 135.16, 135.55, 136.23, 139.85, 140.53, 140.66, 140.85, 140.95, 141.63, 143.09, 143.7, 144.35, 144.43, 144.67, 145.18, 145.34, 145.74, 145.90, 153.65, 153.89; FAB MS (3-nitrobenzyl alcohol matrix) shows a cluster of peaks at 1195–1197 amu (calcd for $C_{80}H_{90}N_8O_2{\cdot}H^+$ 1196); UV–vis λ_{max} (log ϵ) 415 (5.71), 510 (4.71), 540 (4.32), 577 (4.35), 627 (3.78). Anal. Calcd for $C_{80}H_{90}N_8O_2$: C, 80.36; H, 7.59; N, 9.38. Found: C, 80.26; H, 7.70; N, 9.18. When the first red band of the above preparation (containing $Cu_2{\cdot}$**1**) was demetalated and worked up in the same fashion as for $H_4{\cdot}$**12**, a reddish band appeared on the silica gel column which ran

slightly faster than H_4·**1**. This reddish band was collected, passed through another silica gel column ($CHCl_3$ eluent), concentrated, and recrystallized from $CHCl_3$/hexane to give CuH_2·**1** (10 mg) as a red flocculent solid: FAB HRMS (3-nitrobenzyl alcohol matrix) *m/e* calcd for $C_{74}H_{85}N_8$·Cu 1148.61931, found 1148.61450 (−4.2 ppm).

1-[5-[2,8,12,18-Tetraethyl-15-(2,5-dimethoxyphenyl)-3,7,13,17-tetramethylporphyrinyl]]-4-[5-(13,17-di-*n*-butyl-2,8-diethyl-3,7,12,18-tetramethylporphyrinyl)]benzene (H_4·13). Dialdehyde **36** (2.01 g, 4.77 mmol) and dialdehyde **33** (1.16 g, 4.77 mmol) were dissolved in hot THF (150 mL) in a 1-L round-bottomed flask and the solution was diluted to 900 mL with methanol. The α-free dipyrromethane **40** (2.55 g, 4.77 mmol) was then added, and the solution was bubbled with N_2 for 5 min. Perchloric acid (10 mL) was then pipetted in, and the flask was stoppered and shaken vigorously for 1 min and placed in the dark for 24–48 h. The reaction mixture was then worked up as described above for the synthesis of H_4·**12**. In this case, the initial filtration removed undissolved Cu_2·**2**, and again three bands, corresponding to Cu_2·**2**, Cu_2·**13**, and Cu_2·**6**, appeared during the subsequent chromatography (silica, 1/1 v/v CCl_4/$CHCl_3$ eluent). The second red band was collected, concentrated, passed through another similar column, and demetalated by the procedure given above. Chromatographic purification of the resulting free-base was carried out on a 3 × 50 cm silica column (1% MeOH/$CHCl_3$ eluent). Collection of the major band and recrystallization from chloroform/hexane gave H_4·**13** (150 mg, 2.6 %) as a lustrous purple powder. Collection of the third major band, followed by demetalation and standard purification also yielded 140 mg (2.3%) of H_4·**6**. For H_4·**13**: ^{1}H NMR δ −2.73 (s, 1 H, NH), −2.95 (s, 1 H, NH), −1.85 (s, 1 H, NH), −1.97 (s, 1 H, NH), 1.17 (t, 6 H, $CH_2CH_2CH_2CH_3$), 1.7–2.0 (m, 10 H, CH_2CH_3 and $CH_2CH_2CH_2CH_3$), 2.33 (q, 4 H, $CH_2CH_2CH_2CH_3$), 2.67 (s, 6 H, CH_3), 3.19 (s, 6 H, CH_3), 3.22 (s, 6 H, CH_3), 3.70 (s, 6 H, CH_3), 3.72 (s, 3 H, OCH_3), 3.90 (s, 3 H, OCH_3), 4.08 (t, 4 H, CH_2CH_3), 4.16 (q. 4 H, $CH_2CH_2CH_2CH_3$), 7.29–7.40 (m, 3 H, $C_6H_3(OCH_3)_2$), 8.59 (dd, 4 H, $(porph)_2$-phenyl), 9.96 (s, 1 H, meso), 10.27 (s, 2 H, meso), 10.33 (s, 2 H, meso): ^{13}C NMR δ 11.35, 13.17, 13.77, 16.99, 17.16, 19.61, 19.72, 22.76, 25.88, 34.86, 55.80, 95.42, 96.24, 96.30, 111.89, 113.34, 114.95, 117.51, 118.6, 120.24, 132.0, 133.24, 133.36, 134.91, 135.34, 135.80, 139.93, 140.48, 140.77, 141.42, 142.23, 143.47, 143.87, 144.15, 144.20, 144.81, 145.33, 145.50, 145.85; FAB MS (glycerol, oxalic acid matrix) shows a cluster of peaks centered around 1225 amu (calcd for $C_{82}H_{94}N_8O_2$·H^+ 1224); UV–vis λ_{max} (log ε) 416 (5.79), 508 (4.73), 539 (4.24), 575 (4.32), 625 (3.64). Anal. Calcd for $C_{82}H_{94}N_8O_2$: C, 80.49; H, 7.74; N, 9.16. Found: C, 80.33; H, 7.50; N, 9.17.

1-[5-[2,8,12,18-Tetraethyl-15-(2,5-dihydroxyphenyl)-3,7,13,17-tetramethylporphyrinyl]]-3-[5-(2,8-diethyl-3,7,12,18-tetramethyl-13,17-di-*n*-propylporphyrinyl)]benzene (H_4·14). The dimethoxy protected gable monohydroquinone H_4·**12** (290 mg, 0.243 mmol) was dissolved in dry dichloromethane (18 mL) in a 50-mL round-bottomed flask equipped with a side arm and a stir bar. Nitrogen was gently blown in through the side arm. BBr_3 (2 mL) was added to the stirred solution. The flask was promptly stoppered, covered with aluminum foil, and stirred for 3 h. The flask was then unwrapped and the contents diluted to 40 mL with dichloromethane. The excess BBr_3 was quenched by the cautious dropwise addition of methanol (*Caution! Violently Exothermic!*), and the solution was then poured into aqueous K_2CO_3 (5%, 50 mL). After it was stirred for 5–10 min, the organic layer was separated and the aqueous layer further extracted with dichloromethane (2 × 15 mL). The organic layers were combined, washed with water (2 × 40 mL), dried over Na_2SO_4, and taken to dryness on a rotary evaporator to give the crude hydroquinone H_4·**14**, which in general was converted directly to the quinone H_4·**9** without further purification (see below). This crude material could, however, be purified by column chromatography on silica gel (5% MeOH/$CHCl_3$ eluent), followed by recrystallization from 5% methanolic $CHCl_3$/hexane to give pure H_4·**14** as a purple microcrystalline powder (175 mg, 62%): ^{1}H NMR δ −2.95 (br s, 2 H, NH), −2.15 (br s, 2 H, NH), 0.86 (t, 6 H, $CH_2CH_2CH_3$), 1.22 (t, 6 H, CH_2CH_3), 1.70 (t, 6 H, CH_2CH_3), 1.72 (t, 6 H, CH_2CH_3), 2.26 (sextuplet, 4 H, $CH_2CH_2CH_3$), 2.62 (s, 6 H, CH_3), 3.07 (s, 12 H, CH_3), 3.54 (s, 6 H, CH_3), 3.93–4.02 (m, 16 H, CH_2CH_3) and $CH_2CH_2CH_3$), 7.15 (s, 1 H, hydroquinone phenyl H-6), 7.89 (s, 1 H, phenyl H-2), 8.28 (t, 1 H, phenyl H-5), 8.83 (d, 2 H, hydroquinone phenyl H-3, H-4), 8.95 (d, 2 H, phenyl H-4 and H-6), 9.80 (s, 1 H, "distal" meso H-15), 10.05 (s, 2 H, "distal" meso H-10 and H-20), 10.14 (s, 2 H, "proximal" meso H-10 and H-20); ^{13}C NMR δ 11.50, 13.17, 14.23, 16.96, 17.13, 17.17, 17.22, 19.63, 19.78, 25.89, 28.21, 29.53, 95.83, 96.55, 99.23, 109.50, 109.55, 116.48, 117.26, 117.70, 120.02, 125.33, 127.88, 133.35, 133.43, 134.98, 135.13, 135.99, 136.22, 139.90, 140.11, 140.82, 141.07, 141.82, 144.38, 144.72, 144.85, 145.44, 145.72, 149.20, 150.22; FAB MS (glycerol/oxalic acid) shows a cluster of peaks at 1166.8–1171.8 amu (calcd for $C_{78}H_{86}N_8O_2$·H^+ *m/e* = 1166.7).

1-[5-[15-[2′-(1′,4′-Benzoquinonyl)]-2,8,12,18-tetraethyl-3,7,13,17-tetramethylporphyrinyl]]-3-[5-(2,8-diethyl-3,7,12,18-tetramethyl-13,17-di-*n*-propylporphyrinyl)]benzene (H_4·10). The above hydroquinone (H_4·**14**) (175 mg, 0.15 mmol) was dissolved in 30 mL of 1% methanol/$CHCl_3$ containing a trace of triethylamine (TEA). DDQ (100 mg, 0.44 mmol) was then added, the solution was stirred for 5 min, and it was then loaded onto a 2 × 50 cm silica gel column and eluted (1% methanol/$CHCl_3$). The fastest moving dark band was collected and recrystallized, first from $CHCl_3$/MeOH and then from $CHCl_3$/hexane, to give the product as a fluffy brown solid (quantitative): ^{1}H NMR δ −2.9 to −3.1 (d, 2 H, pyrrole NH), −2.05 to −2.2 (br s, 2 H, pyrrole NH), 1.26 (t, 6 H, $CH_2CH_2CH_3$), 1.77 (m, 18 H, CH_2CH_3), 2.30 (m, 4 H, $CH_2CH_2CH_3$), 3.09 (s, 18 H, CH_3), 3.59 (s, 6 H, CH_3), 3.99 (m, 16 H, CH_2CH_3), 7.29 (d, 1 H, quinone H), 7.32 (br, 2 H, quinone H), 7.95 (br s, 1 H, $(porph)_2$-phenyl), 8.29 (t, 1 H, $(porph)_2$-phenyl), 8.95 (d, 2 H, $(porph)_2$-phenyl), 9.83 (s, 1 H, meso), 10.10 (s, 2 H, meso), 10.15 (s, 2 H, meso); ^{13}C NMR δ 11.8, 14.2, 16.2, 17.0, 17.3, 20.0, 26.1, 28.2, 29.7, 95.9, 96.7, 97.3, 106.2, 117.8, 118.3, 125.4, 133.1, 133.4, 133.5, 135.2, 135.4, 136.3, 137.2, 137.8, 139.4, 139.9, 140.1, 141.2, 141.3, 141.8, 142.2, 143.7, 144.6, 145.0, 145.1, 145.5, 146.0, 146.2, 150.0, 187.1, 188.8; FAB MS (glycerol, oxalic acid matrix) shows a cluster of peaks at 1165.9–1171.9 amu (calcd for $C_{78}H_{84}N_8O_2$·H^+ 1165.7); UV–vis λ_{max} (log ε) 415.5 (5.59), 508.5 (4.60), 541 (4.31), 577 (4.24), 628 (3.83). Anal. Calcd for $C_{78}H_{84}N_8O_2$·H_2O: C, 79.15; H, 7.32; N, 9.47. Found: C, 79.21; H, 7.20; N, 9.37. For Zn_2·**10**: UV–vis λ_{max} (log ε) 407 (5.57), 424 (5.52), 543 (4.57), 575 (4.43).

1-[5-[2,8,12,18-Tetraethyl-15-(2,5-dihydroxyphenyl)-3,7,13,17-tetramethylporphyrinyl]]-4-[5-(13,17-di-*n*-butyl-2,8-diethyl-3,7,12,18-tetramethylporphyrinyl)]benzene (H_4·15). The dimethoxy protected material H_4·**13** (125 mg, 0.1 mmol) was deprotected by a procedure identical with that used to obtain H_4·**14** to give H_4·**15** in 76% yield: ^{1}H NMR δ 1.08 (t, 6 H, $CH_2CH_2CH_2CH_3$), 1.8–1.9 (m, 10 H, CH_2CH_3 and $CH_2CH_2CH_2CH_3$), 2.23 (q, 4 H, $CH_2CH_2CH_2CH_3$), 2.70 (s, 6 H, CH_3), 3.05 (s, 6 H, CH_3), 3.08 (s, 6 H, CH_3), 3.61 (s, 6 H, CH_3), 3.9–4.2 (m, 16 H, CH_2CH_3 and $CH_2CH_2CH_2CH_3$), 7.12 (s, 1 H, -H4 of $C_6H_3(OH)_2$), 7.26 (s, 1 H, -H3 of $C_6H_3(OH)_2$), 8.36 (dd, 4 H, $(porph)_2$-phenyl), 8.43 (s, 1 H, -H6 of $C_6H_3(OH)_2$), 9.87 (s, 1 H, meso), 10.21 (s, 2 H, meso), 10.30 (s, 2 H, meso); FAB MS (glycerol/oxalic acid matrix) shows a cluster of peaks from 1195–1198 amu (calcd for $C_{80}H_{90}N_8O_2$·H^+ 1195).

1-[5-[15-[2′-(1′,4′-Benzoquinonyl)]-2,8,12,18-tetraethyl-3,7,13,17-tetramethylporphyrinyl]]-4-[5-(13,17-di-*n*-butyl-2,8-diethyl-3,7,12,18-tetramethylporphyrinyl)]benzene (H_4·11). The hydroquinone H_4·**15** was oxidized to the quinone H_4·**11** in near quantitative yield by the same procedure used to prepare H_4·**10**: ^{1}H NMR δ −2.7 to −3.0 (d, 2 H, pyrrole NH), −1.85 to −2.05 (br s, 2 H, pyrrole NH), 1.16 (t, 6 H, $CH_2CH_2CH_2CH_3$), 1.80 (m, 4 H, $CH_2CH_2CH_2CH_3$), 1.95 (m, 18 H, CH_2CH_3), 2.32 (m, 4 H, $CH_2CH_2CH_2CH_3$), 3.19 (s, 18 H, CH_3), 3.69 (s, 6 H, CH_3), 4.0–4.2 (m, 16 H, $CH_2CH_2CH_3$ and $CH_2CH_2CH_2CH_3$), 7.3–7.4 (m, 3 H, quinone H), 8.45 (dd, 4 H, $(porph)_2$-phenyl), 9.95 (s, 1 H, meso), 10.26 (s, 2 H, meso), 10.34 (s, 2 H, meso); ^{13}C NMR δ 11.8, 14.2, 16.3, 17.4, 17.6, 17.7, 17.8, 20.0, 20.1, 23.1, 26.2, 35.3, 96.8, 97.5, 106.4, 118.8, 119.3, 125.5, 128.2, 133.3, 133.4, 133.5, 133.9, 134.0, 135.6, 136.0, 136.3, 137.2, 137.9, 139.5, 140.4, 141.2, 141.3, 141.7, 141.8, 142.8, 143.8, 144.7, 144.9, 145.0, 145.7, 146.1, 150.0, 187.3, 189.0; FAB MS (glycerol/oxalic acid matrix) shows a cluster of peaks from 1192.6–1199.6 amu (calcd for $C_{80}H_{88}N_8O_2$·H^+ 1192.7); UV–vis λ_{max} (log ε) 414.5 (5.60), 507 (4.58), 539 (4.24), 573 (4.23), 624 (3.93). Anal. Calcd for $C_{80}H_{88}N_8O_2$: C, 80.5; H, 7.43; N, 9.39. Found: C, 80.32; H, 7.43; N, 9.09. For Zn_2·**11**: UV–vis λ_{max} (log ε) 412sh (5.52), 423 (5.69), 542 (4.66), 574 (4.40).

Monometalations. ZnH_2·1. 1,3-Bis[5-(2,8-Diethyl-3,7,12,18-tetramethyl-13,17-di-*n*-propylporphyrinyl)]benzene (H_4·**1**) (11 mg, 0.010 mmol) was dissolved in 30 mL of $CHCl_3$ in a 50-mL round-bottomed flask equipped with a magnetic stirring bar. Aliquots (10-mL each) of a 0.0055 M solution of zinc acetate in methanol were then added with efficient stirring. The course of the reaction was monitored by TLC (silica gel, developing with 2% MeOH in $CHCl_3$) after each addition. When approximately 1.3 equiv of Zn^{2+} had been added, TLC indicated the absence of appreciable starting material and the presence of two new spots. The faster moving of these (R_f = 0.72) corresponds to Zn_2·**1**; the other to ZnH_2·**1** (R_f = 0.44). Unfortunately, the monozinc complex moves only slightly faster on TLC than the starting free-base (R_f = 0.42). Chromatographic purification on a 1 cm × 25 cm column (silica gel, $CHCl_3$ eluent) followed by recrystallization from $CHCl_3$/hexanes thus gave ZnH_2·**1** (4 mg, 34%) contaminated with a small amount of H_4·**1**. Pure ZnH_2·**1** could only be obtained after several repeated chromatography and recrystallization cycles. The ^{1}H NMR spectrum was similar to that of H_4·**1**, except for a reduced integral value for the internal protons at ca. −3 ppm: FAB MS (3-nitrobenzyl alcohol matrix) shows

a cluster of peaks at 1148–1153 amu (calcd for $C_{74}H_{84}N_8Zn{\cdot}H^+$ 1149 and 1151); UV–vis λ_{max} (log ϵ) 407.5 (5.61), 417 (5.60), 506.5 (4.36), 540.5 (4.44), 574.5 (4.35), 627 (3.50).

ZnH_2·2. This complex was obtained from H_4·**2** in 38% yield by the procedure described above for the preparation of ZnH_2·**1**. Again, the monozinc complex (R_f = 0.42) moved considerably more slowly than the bis-zinc complex (R_f = 0.84) but only slightly faster on TLC (silica gel, developing with 1% MeOH in $CHCl_3$) than the free-base (R_f = 0.39). As a result, several chromatographic purification (silica gel, $CHCl_3$, eluent) and recrystallization (from $CHCl_3$/hexanes) cycles were again required to remove the last traces of the starting free-base porphyrin. The ^1H NMR spectrum (see discussion in text) was similar to that of H_4·**2**, except for the reduced integral value in the internal pyrrole region: FAB MS (3-nitrobenzyl alcohol matrix) shows a cluster of peaks at 1205–1208 amu (calcd for $C_{78}H_{92}N_8Zn{\cdot}H^+$ 1205 and 1207); UV–vis λ_{max} (log ϵ) 417 (5.60), 508 (4.27), 539 (4.42), 575 (4.24).

ZnH_2·3. This complex was obtained in impure form from H_4·**3** by a procedure identical with that described above for the preparation of ZnH_2·**1**. In this case, however, the desired monozinc complex (R_f = 0.38), the bis-zinc complex (R_f = 0.55) and starting free-base (R_f = 0.37) were not well separated on TLC (silica gel, developing with 1% MeOH in $CHCl_3$). As a result, chromatographic purification (silica gel, $CHCl_3$, eluent) and recrystallization (from $CHCl_3$/hexanes) served only to remove the bis-zinc complex; the sample of ZnH_2·**3** used for NMR studies (c.f. Figure 10) was estimated to contain ca. 20% H_4·**3** as an impurity: FAB MS (3-nitrobenzyl alcohol matrix) shows a cluster of peaks at 1308–1313 amu (calcd for $C_{82}H_{80}N_8O_4Zn{\cdot}H^+$ 1305 and 1307), as well as at 1247–1251 amu corresponding to the free base H_4·**3**.

ZnH_2·10. This complex was obtained directly from H_4·**10** by a modification of the procedure described above for the preparation of ZnH_2·**1**: The starting free-base porphyrin (100 mg, 0.086 mmol) was dissolved in 400 mL of pure $CHCl_3$ and titrated with 0.1-mL aliquots of a 0.0055 M solution of zinc acetate with good stirring. After the addition of roughly 1.3 equiv, TLC (silica gel, developing with 2% MeOH in $CHCl_3$) indicated an approximately 1:1 mixture of ZnH_2·**10** (R_f = 0.65) and Zn_2·**10** (R_f = 0.94) and very little remaining H_4·**10** (R_f = 0.51). After the material was washed with water and dried over Na_2SO_4, chromatographic purification (silica gel, $CHCl_3$, eluent) and recrystallization (from $CHCl_3$/hexanes) gave pure ZnH_2·**10** (38 mg, 36%) uncontaminated with either the starting free-base or bis-zinc compounds. The ^1H NMR spectrum was similar to that of H_4·**10**, with the exception of the internal pyrrole region (see discussion in results section): FAB MS (3-nitrobenzyl alcohol matrix) shows a cluster of peaks at 1228–1235 amu (calcd for $C_{78}H_{82}N_8O_2Zn{\cdot}H^+$ 1227 and 1229); UV–vis λ_{max} (log ϵ) 408 (5.51), 419 (5.50), 509 (4.37), 542 (4.45), 576 (4.33).

ZnH_2·11. This complex was obtained from H_4·**11** in 48% yield by using the same procedure used to prepare ZnH_2·**10** from H_4·**10**. Again, the monozinc complex (R_f = 0.75) was well separated on TLC (silica gel, developing with 1% MeOH in $CHCl_3$) from the bis-zinc complex (R_f = 0.87) and starting free-base (R_f = 0.64) porphyrin and could be readily purified by chromatography on silica gel ($CHCl_3$, eluent), followed by recrystallization (from $CHCl_3$/hexanes). The ^1H NMR spectrum was similar to that of H_4·**11**, with the exception of the internal pyrrole region as mentioned in the results section: FAB MS (3-nitrobenzyl alcohol matrix) shows a cluster of peaks at 1255–1262 amu (calcd for $C_{80}H_{88}N_8O_2Zn{\cdot}H^+$ 1255 and 1257); UV–vis λ_{max} (log ϵ) 417 (5.62), 509 (4.31), 539 (4.40), 573 (4.29).

H_2Zn·10. The starting free-base hydroquinone porphyrin H_4·**14** (100 mg, 0.086 mmol) was dissolved in 400 mL pure $CHCl_3$ and titrated with 0.1-mL aliquots of 0.0055 M zinc acetate with good stirring. After the addition of roughly 1.3 equiv, TLC (silica gel, developing with 2% MeOH in $CHCl_3$) indicated an approximately 1:1 mixture of H_2Zn·**14** (R_f = 0.33) and Zn_2·**14** (R_f = 0.97) and very little remaining H_4·**14** (R_f = 0.26). Following an aqueous workup, chromatographic purification (silica gel, $CHCl_3$, eluent) gave moderately pure ZnH_2·**14** contaminated with a trace of starting free-base H_4·**14**. This crude product was not isolated but was immediately dissolved in 30 mL of 1% methanol/$CHCl_3$ containing a trace of TEA and oxidized with DDQ (100 mg, 0.44 mmol). After the solution was stirred for 5 min, it was loaded onto a 5 × 100 cm silica gel column and eluted with pure $CHCl_3$. The slowest moving dark band was collected and recrystallized from $CHCl_3$/hexane to give H_2Zn·**10** as a fluffy brown solid (45 mg, 43%). Interestingly, this monometalated product (R_f = 0.45) moves *slower* on TLC (silica gel, 2% MeOH in $CHCl_3$) than either the free-base quinone H_4·**10** (R_f = 0.51) or its chelate ZnH_2·**10** (R_f = 0.65). The ^1H NMR spectrum was similar to that of H_4·**10**, with the exception of the internal pyrrole region (see discussion in results section): FAB MS (3-nitrobenzyl alcohol matrix) shows a cluster of peaks at 1223–1230 amu (calcd for $C_{78}H_{82}N_8O_2Zn{\cdot}H^+$ 1227 and 1229); UV–vis λ_{max} (log ϵ) 410 (5.48), 422 (5.52), 507 (4.36), 543 (4.43), 577 (4.30).

H_2Zn·11. This complex was obtained from H_4·**15** in 45% yield by the same procedure used to prepare H_2Zn·**10** from H_4·**14**. Again, the final monometalated quinone product H_2Zn·**11** migrates slower on TLC (R_f = 0.53, silica gel, 2% MeOH/$CHCl_3$) than the free-base H_4·**11** (R_f = 0.64) or the isomeric complex ZnH_2·**11** (R_f = 0.75). The ^1H NMR spectrum was similar to that of H_4·**10**, with the exception of the internal pyrrole region (see above): FAB MS (3-nitrobenzyl alcohol matrix) shows a cluster of peaks at 1253–1258 amu (calcd for $C_{80}H_{86}N_8O_2Zn{\cdot}H^+$ 1255 and 1257); UV–vis λ_{max} (log ϵ) 420 (5.61), 507 (4.34), 540 (4.44), 572 (4.30), 624 (3.86).

Acknowledgment. This work was supported by the Robert A. Welch Foundation (Grant F-1018 to J.L.S.), the National Science Foundation (PYI Award, 1986 to J.L.S.), and the National Institutes of Health (Grant No. HL 13157 to J.A.I. and Grant No. GM 41657 to J.L.S.). We thank Profs. M. Momenteau and F. A. Walker for their help in interpreting the temperature dependent ^1H NMR spectra, Azadeh Mozaffari for synthetic assistance, and Prof. J.-P. Sauvage for sharing results prior to publication.

Supplementary Material Available: Synthetic details for the preparation of precursors **24**–**33**, **41**, and **42**, tables of selected bond distances and angles, positional and isotropic thermal parameters for hydrogen atoms, and positional and equivalent isotropic thermal parameters for non-hydrogen atoms for H_2·**20**, Cu_2·**5**, and Cu_2·**9**, table of mean lifetimes for the bridging phenyl protons for H_4·**4** and H_4·**6**, temperature-dependent proton NMR spectra for compounds H_4·**11** and H_4·**13**, and Arrhenius plots for proton exchange in compounds H_4·**6** and H_4·**4** (46 pages); tables of structure factors ($10|F_o|$ vs $10|F_c|$) for H_2·**20**, Cu_2·**5**, and Cu_2·**9** (105 pages). Ordering information is given on any current masthead page.